

# Gli Protein Activity Is Controlled by Multisite Phosphorylation in Vertebrate Hedgehog Signaling

Pawel Niewiadomski,<sup>1,2,5,\*</sup> Jennifer H. Kong,<sup>4,7</sup> Robert Ahrends,<sup>3,6,7</sup> Yan Ma,<sup>1,2</sup> Eric W. Humke,<sup>1,2,8</sup> Sohini Khan,<sup>1,2</sup> Mary N. Teruel,<sup>3</sup> Bennett G. Novitch,<sup>4</sup> and Rajat Rohatgi<sup>1,2,\*</sup>

<sup>1</sup>Department of Medicine, Stanford University School of Medicine, Stanford, CA 94305, USA

<sup>2</sup>Department of Biochemistry, Stanford University School of Medicine, Stanford, CA 94305, USA

<sup>3</sup>Department of Chemical and Systems Biology, Stanford University School of Medicine, Stanford, CA 94305, USA

<sup>4</sup>Department of Neurobiology, Eli and Edythe Broad Stem Cell Research Center, David Geffen School of Medicine at UCLA, Los Angeles, CA 90095, USA

<sup>5</sup>Department of Cell Biology, Nencki Institute of Experimental Biology, 02-093 Warsaw, Poland

<sup>6</sup>Laboratory of Quantitative Systems Analysis, Leibniz-Institute for Analytical Sciences (ISAS) e.V., 44227 Dortmund, Germany

<sup>7</sup>These authors contributed equally to this work

<sup>8</sup>Present address: Genentech, Inc., Early Clinical Development, 1 DNA Way, M/S 442, South San Francisco, CA 94080, USA

\*Correspondence: [p.niewiadomski@nencki.gov.pl](mailto:p.niewiadomski@nencki.gov.pl) (P.N.), [rrohathgi@stanford.edu](mailto:rrohathgi@stanford.edu) (R.R.)

<http://dx.doi.org/10.1016/j.celrep.2013.12.003>

This is an open-access article distributed under the terms of the Creative Commons Attribution-NonCommercial-No Derivative Works License, which permits non-commercial use, distribution, and reproduction in any medium, provided the original author and source are credited.

## SUMMARY

Gli proteins are transcriptional effectors of the Hedgehog (Hh) pathway in both normal development and cancer. We describe a program of multisite phosphorylation that regulates the conversion of Gli proteins into transcriptional activators. In the absence of Hh ligands, Gli activity is restrained by the direct phosphorylation of six conserved serine residues by protein kinase A (PKA), a master negative regulator of the Hh pathway. Activation of signaling leads to a global remodeling of the Gli phosphorylation landscape: the PKA target sites become dephosphorylated, while a second cluster of sites undergoes phosphorylation. The pattern of Gli phosphorylation can regulate Gli transcriptional activity in a graded fashion, suggesting a phosphorylation-based mechanism for how a gradient of Hh signaling in a morphogenetic field can be converted into a gradient of transcriptional activity.

## INTRODUCTION

The Hedgehog (Hh) pathway is an evolutionarily conserved signaling system that plays a central role in embryogenesis and adult tissue homeostasis. Its misregulation leads to developmental defects and to cancers of the skin and the brain (Briscoe and Théron, 2013; Hahn et al., 1996). The Gli (*Glioblastoma*) transcription factors in vertebrates control the Hh gene expression program (Hui and Angers, 2011). Despite the importance of Gli proteins in development, regeneration, and cancer, the mechanism by which they acquire the ability to activate target genes has remained enigmatic.

Among the three mammalian Gli proteins, Gli2 and Gli3 are the first responders to the Hh signal. Once activated, Gli2/3 then induce the expression of Gli1, which acts as an amplifier of the response. Gli2/3 can perform two opposing functions at target promoters (Figure 1A; reviewed in Hui and Angers, 2011). When the pathway is off, Gli2/3 proteins are converted into truncated repressor forms (hereafter abbreviated GliR), which inhibit target gene transcription. When the Hh ligand is received, GliR production is blocked and Gli2/3 proteins are converted into transcriptional activators (hereafter abbreviated GliA). In the nucleus, the balance between GliR and GliA shapes the Hh response. Between these two extremes, a substantial fraction of Gli2/3 remains in the cytoplasm in a transcriptionally inactive state (Humke et al., 2010). Quantitative changes in the GliR/GliA ratio can lead to developmental defects in humans, underscoring the point that the precise level of Gli activity is often critical for the sophisticated patterning events regulated by Hh signaling during development (Hill et al., 2007; Kang et al., 1997; Wang et al., 2000).

GliR and GliA production are both controlled by the seven-transmembrane protein Smoothed (Smo; Figure 1A). Upon Hh ligand reception by Patched (Ptc), Smo accumulates in a microtubule-based protrusion of the cell membrane known as the primary cilium (Corbit et al., 2005). Through an unknown mechanism, ciliary Smo inhibits GliR formation and induces the transport of Gli proteins to the tips of cilia (Kim et al., 2009; Wen et al., 2010), where they dissociate from the negative regulator Suppressor of Fused (SuFu; Humke et al., 2010; Tukachinsky et al., 2010). Thereupon, Glis translocate into the nucleus and activate target genes. Nuclear Gli proteins are characterized by a short half-life and reduced mobility on SDS-PAGE gels caused by a distinct phosphorylation event, hereafter referred to as “hyperphosphorylation” (Humke et al., 2010).

The mechanistic details of the interaction between Smo and Gli proteins are not understood. Several lines of evidence point to protein kinase A (PKA) as a key regulator of the Hh signal

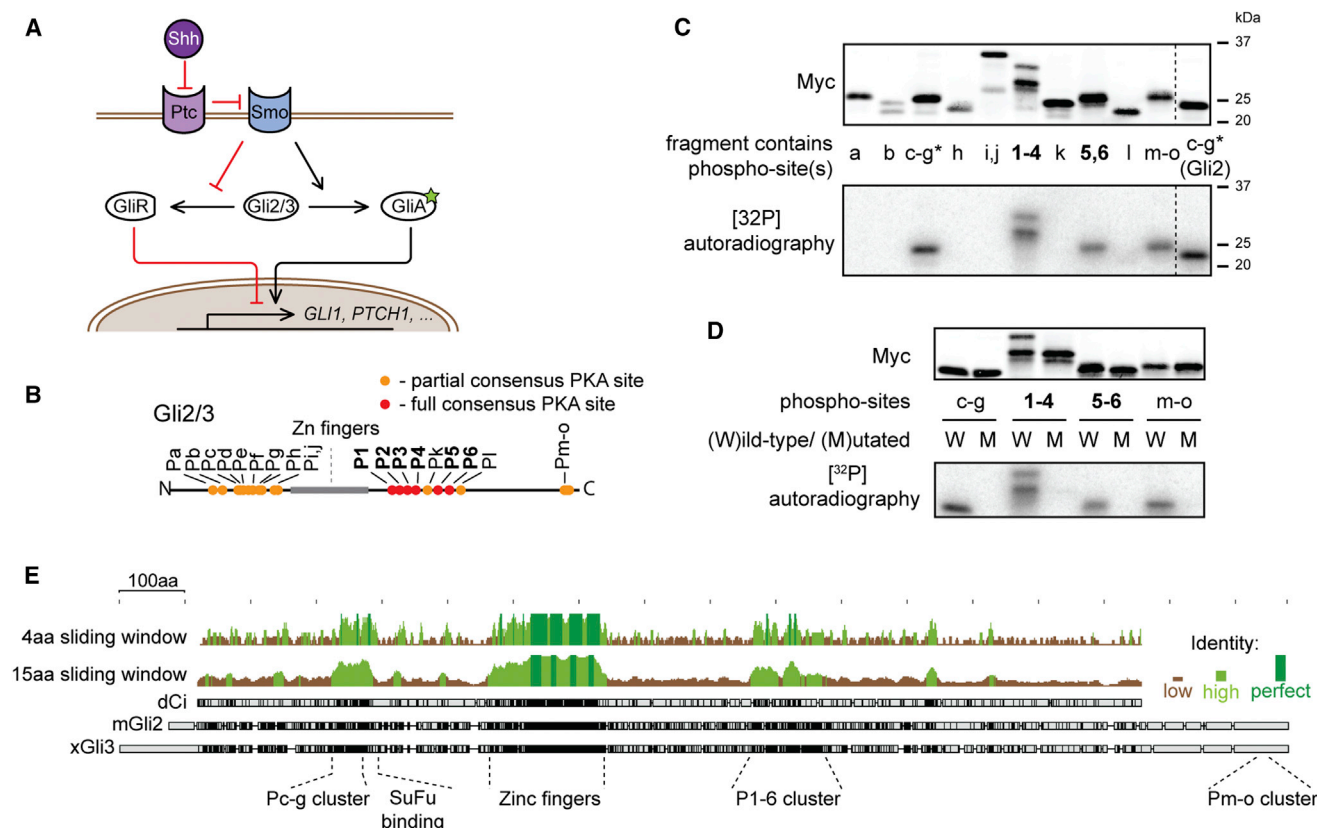


**Figure 1. PKA Phosphorylates Both Full and Partial Consensus Sites on Gli2/3 In Vitro**

(A) Schematic representation of Gli2/3 regulation by Hh signaling. Active Smo induces the formation of GliA and suppresses the production of the truncated GliR. (B) Location of the full (red dots; P1–6) and partial consensus (orange dots; Pa–o) PKA target sites that are conserved in both mouse and human Gli2 and Gli3. (C) In vitro PKA phosphorylation of Myc-tagged Gli3 fragments containing the indicated target sites. An anti-myc immunoblot (top) shows total protein levels of each fragment in the assay and the autoradiogram (bottom) shows  $^{32}\text{P}$  incorporation. The P-c-g (\*) fragment was tested for both Gli3 and Gli2 since only the former contains an additional PKA consensus target sequence. (D) S/T residues presumed to be PKA targets were mutated in Gli3 fragments containing sites P-c-g, P1–4, P5,6, and Pm–o. Wild-type (W) or mutant (M) fragments were subjected to in vitro phosphorylation as in (C). (E) Protein sequences of *Drosophila* Ci, mouse Gli2, and *Xenopus* Gli3 were aligned using the Geneious algorithm and the degree of conservation of protein sequences was plotted for either a 4-amino-acid or 15-amino-acid sliding window.

downstream of Smo (Fan et al., 1995; Hammerschmidt et al., 1996; Hynes et al., 1995; Jiang and Struhl, 1995; Lepage et al., 1995; Li et al., 1995; Niewiadomski et al., 2013; Pan and Rubin, 1995; Strutt et al., 1995; Tuson et al., 2011). Pharmacological activation of PKA completely blocks Hh signaling, even in the presence of the Hh ligand or a Smo agonist. Conversely, genetic ablation of PKA shifts the GliR/GliA balance strongly in favor of GliA. This leads to full ligand-independent activation of Hh target genes, manifested as complete ventralization of the embryonic neural tube in mutant mice (Tuson et al., 2011). These data clearly identify PKA as a negative regulator of Gli function, but on a molecular level, our understanding of how Gli proteins are influenced by PKA remains incomplete.

The mechanism by which PKA promotes GliR has been elucidated in detail, guided by studies of the *Drosophila* Gli homolog *cubitus interruptus* (Ci; Aza-Blanc et al., 1997; Méthot and Basler, 1999; Price and Kalderon, 1999; Wang et al., 1999). PKA can phosphorylate Gli2/3 at six conserved serine residues (P1–6) located on

the carboxyterminal side of the DNA binding Zn-finger domain (Figure 1B; Wang et al., 2000). The phosphorylation of the first four of these residues (P1–4) by PKA initiates a pathway that leads to the partial processing of full-length Glis into GliR fragments by the proteasome (Pan et al., 2009; Wang et al., 1999); the function of the last two phosphorylation sites (P5,6) is unknown.

PKA plays an equally important but much less well-understood role in suppressing Gli2/3A. Loss of phosphorylation at sites P1–4, which regulates GliR production, does not seem to be sufficient for this activation step. Transgenic mice harboring nonphosphorylatable serine-to-alanine mutations in P1–4 of Gli2 do not show the developmental phenotypes expected if Gli2 was fully activated (Pan et al., 2009). Importantly, the neural tube of these animals, in contrast to animals lacking PKA activity, is not strongly ventralized. Thus, PKA must inhibit Gli2 activation by phosphorylating sites other than P1–4.

Here, we elucidate the mechanism by which PKA inhibits the production of GliA. PKA uses distinct phosphorylation patterns

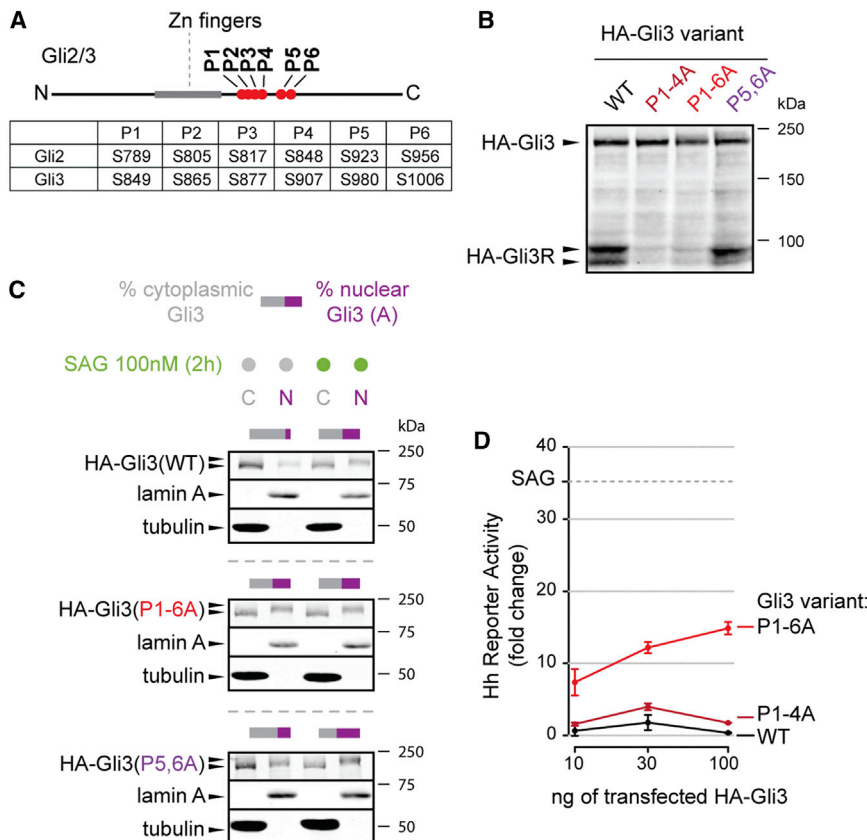


**Figure 2. The P1-6 Cluster Regulates the Balance between Gli3 Activator and Gli3 Repressor**

(A) Location of sites P1-6 on mouse Gli2 and Gli3. (B) An anti-HA immunoblot reveals the relative levels of full-length and repressor Gli3 in whole-cell extracts from NIH/3T3 Flp-In cells stably expressing HA-tagged Gli3 variants.

(C) Distribution of full-length HA-Gli3 variants in the nuclear (N) and cytoplasmic (C) fractions of NIH/3T3 Flp-In cells left untreated or treated with SAG (100 nM, 2 hr). In this and subsequent figures, lamin A and tubulin serve as control nuclear and cytoplasmic proteins to assess the quality of the fractionation and bars above each blot represent the relative abundance of HA-Gli3 in the cytoplasmic (gray) and nuclear (purple) fractions as determined by quantitative immunoblotting. Figure S2B compiles data from five repeats of such an experiment.

(D) Activation of a luciferase-based Hh reporter gene in NIH/3T3 cells (untreated with any Hh agonists) transiently transfected with the reporter construct in combination with the indicated Gli3 variants. Values were normalized to reporter induction seen with an empty plasmid (control). Dashed gray line shows the level of reporter activation seen with SAG (100 nM; 24 hr) in cells transfected with a control vector. See also Figure S2C. Error bars indicate SD from three independent transfections.

to regulate GliR and GliA; phosphorylation of P1-4 is sufficient for GliR production, while the inhibition of GliA formation is dependent on all six sites from the P1-6 cluster. Smo activation reduces phosphorylation of P1-6, showing that Hh signaling wields direct control over phosphorylation at these sites. We also find that P1-6 dephosphorylation allows the phosphorylation of Gli2 at a distinct cluster of sites, which plays a positive role in Hh signaling. We propose that remodeling of the phosphorylation landscape of Gli2/3 proteins controls the transcriptional output of Hh signaling and discuss the implications of this model for the role of Hh as a morphogen in development.

## RESULTS

### PKA Phosphorylates Gli2/3 at Multiple Sites In Vitro

Previous work has implicated PKA both in GliR formation and in GliA inhibition (Hammerschmidt et al., 1996; Pan et al., 2009; Tuson et al., 2011; Wang et al., 1999, 2000), but the biochemical mechanism by which PKA blocks GliA formation was unknown. We hypothesized that PKA suppresses the formation of GliA by direct phosphorylation of Gli2/3. In order to identify putative inhibitory PKA target sites on Gli2/3, we looked for full consensus sites (R or K present at positions -2 and -3 from the S or T) and partial consensus sites (R or K only present at either position -2 or position -3 from the S or T) that were conserved among human and mouse Gli2 and Gli3 and were located outside the DNA-binding zinc finger domain (Figure S1A). In addition to the

full consensus sites (P1-6) described previously (Pan et al., 2009; Price and Kalderon, 1999; Wang et al., 2000), we identified 15 partial consensus sites (hereafter called Pa-o; Figures 1B and S1B). Myc-tagged fragments of Gli3 containing various subsets of these sites were tested as PKA substrates using an in vitro kinase assay. Four fragments containing sites P1-4, P5,6, Pc-g, and Pm-o could be phosphorylated by PKA (Figures 1C and 1D). Interestingly, both the P1-6 and the Pc-g clusters are located in regions of Gli2/3 that are strongly conserved among the *Drosophila*, *Xenopus*, and mouse proteins (Figure 1E).

### PKA Target Sites P1-6 Regulate Gli3 Repressor and Activator Functions

We first analyzed the six sites in the P1-6 cluster, which had previously been identified as PKA targets (Riobó et al., 2006; Wang et al., 2000; Figure 2A). We decided to study P1-6 in the context of both Gli3 and Gli2, since Gli3 is the major repressor (Gli3R) and Gli2 the major activator (Gli2A) in most tissues. To understand the role of specific sites within the P1-6 cluster in regulating the GliR/GliA balance, we made nonphosphorylatable alanine mutants of P1-4 (P1-4A), P5 and P6 (P5,6A), or of the entire P1-6 cluster (P1-6A) in Gli2 and Gli3. Since Gli proteins fail to be regulated by Hh signaling when overproduced in cells (Humke et al., 2010), we sought to evaluate these Gli mutants under endogenous expression levels. To that end, we stably expressed hemagglutinin (HA)-tagged Gli2/3 (HA-Gli2/3) mutants in NIH/3T3 fibroblasts using the Flp-In system, in which an expression

construct is introduced as a single-copy insertion into a defined locus in the genome by Flp-mediated recombination (Torres et al., 2009; Zhou et al., 2010). The Flp-In system allowed us to rapidly generate stable cell lines expressing Gli protein variants at near-endogenous (Figure S2A) and roughly equal (Figure 2B) levels.

Starting with Gli3, we verified that a wild-type (WT) HA-Gli3 behaved like its endogenous counterpart. Indeed, HA-Gli3(WT) could be processed into a HA-GliR fragment when expressed using the Flp-In system (Figure 2B). Consistent with previous reports (Pan et al., 2006, 2009; Tempé et al., 2006; Wang and Li, 2006), mutation of sites P1–4 into alanine was sufficient to block Gli3R formation, as neither Gli3(P1–4A) nor Gli3(P1–6A) was converted into Gli3R. In contrast, Gli3(P5,6A) readily formed Gli3R in unstimulated cells (Figure 2B). Prior reports have implicated all six sites in the P1–6 cluster in GliR formation (Wang et al., 2000), but these studies were based on transient Gli3 overexpression and required stimulation with high doses of forskolin for prolonged periods of time to produce Gli3R. Using experimental conditions that faithfully reflect endogenous Gli3 processing in untreated cells, we find that sites P5 and P6 are not involved in the PKA-dependent truncation of Gli3 into a repressor fragment.

The formation of Hh-induced Gli3A can be experimentally followed by two biochemical events: activated Gli3 translocates into the nucleus and undergoes hyperphosphorylation, which appears as a shift in the apparent molecular weight of Gli proteins on SDS-PAGE gels (Humke et al., 2010). As we have previously described for endogenous Gli3, treatment of cells with the Smo agonist SAG led to the redistribution of HA-Gli3(WT) into the nuclear fraction; nuclear HA-Gli3 also showed the characteristic reduction in electrophoretic mobility indicative of hyperphosphorylation (Figure 2C, top panel, and Figure S2B). In contrast, when all six of the P1–6 sites were simultaneously mutated to alanines, Gli3 accumulated to high levels in the nucleus even in the absence of Hh signaling (Figure 2C, middle panel, and Figure S2B). Saturating concentrations of SAG did not further increase the nuclear accumulation of HA-Gli3(P1–6A), showing that the mutation of these six residues makes Gli3 unresponsive to upstream Hh signals. Alanine mutations only in sites P5 and P6 increased levels of Gli3 in the nucleus seen in the absence of signaling but did not result in maximal nuclear accumulation; HA-Gli3(P5,6A) still moved to the nucleus in response to SAG (Figure 2C, bottom panel, and Figure S2B).

To measure transcriptional activity of the Gli3 mutants, we transiently transfected constructs encoding each protein and measured the activation of an Hh-dependent firefly luciferase reporter gene (Sasaki et al., 1997). Consistent with prior characterization of Gli3 as a weak transcriptional activator (Sasaki et al., 1997), both HA-Gli3(WT) and HA-Gli3(P1–4A) failed to substantially increase Hh-dependent luciferase expression. On the other hand, HA-Gli3(P1–6A) could activate the reporter gene (Figure 2D), confirming the role of P5 and P6 in limiting the ability of Gli3 to activate transcription. Neither HA-Gli3(P1–4A) nor HA-Gli3(P1–6A) could be processed to Gli3R (Figure 2B), and so differences in their ability to activate transcription cannot be attributed differences in Gli3R levels. All six sites in the P1–6 cluster play a role in tuning Gli3 activity, since HA-Gli3(P5,6A)

also demonstrated low levels of transcriptional activity, analogous to that of HA-Gli3(P1–4A) (Figure S2C).

These results suggest that Gli3 may be regulated by graded dephosphorylation. Loss of P1–4 phosphorylation blocks Gli3R repressor formation but is insufficient for the full activation of Gli3. The additional loss of P5,6 phosphorylation is required to achieve complete transformation of Gli3 into Gli3A.

### Sites P1–6 Determine the Transcriptional Activity of Gli2

Since Gli2 is the major transcriptional activator of Hh target genes in most tissues, we made a similar series of mutations in the P1–6 sites of Gli2. While WT HA-Gli2 can activate the Hh reporter in transient overexpression assays (Figure 3A; Sasaki et al., 1999), the Gli2(P1–6A) mutant was significantly more active at all doses tested. The P1–4A and P5,6A mutants of Gli2 showed an intermediate capacity to activate the reporter. Mutation of either P5 or P6 individually in combination with P1–4 also increased activity of Gli2, suggesting that P5 and P6 may be partially redundant (Figure S2D). Conversely, mutation of both sites P5 and P6 to aspartate (P5,6D), a phospho-mimetic mutation, substantially reduced the activating potential of Gli2 (Figure S2D). These results are consistent with an inhibitory role of P1–6 phosphorylation in the activation of Gli2.

To examine Gli2 regulation under physiological expression levels, we turned to Flp-In stable lines carrying HA-tagged Gli2 mutants (Figure S2A). Similar to its effect on Gli3, the P1–6A mutation in HA-Gli2 caused constitutive Hh-independent accumulation in the nucleus, consistent with Gli2(P1–6A) being a fully active molecule (Figure 3B). In order to correlate nuclear accumulation with transcriptional activity, we measured the expression of endogenous *Gli1*, a Hh target gene commonly used as a metric for pathway activity, in these same stable cell lines. In the absence of Hh signaling, Gli1 levels were not elevated in the line expressing HA-Gli2(WT), confirming that this exogenous protein is properly regulated (Figure S2E). To account for differences in expression levels of the HA-Gli2 variants (Figure 3C), we compared their specific activities, calculated as the level of Gli1 induction divided by the protein level of the corresponding HA-Gli2 variant. The specific activities of the mutants fell along a gradient: the HA-Gli2(P1–4A) and HA-Gli2(P5,6A) mutants demonstrated ~3- to 4-fold higher specific activity and the HA-Gli2(P1–6A) mutant displayed ~13-fold higher specific activity compared to HA-Gli2(WT) (Figure 3C). The high level of Gli1 in cells carrying Gli2(P1–6A) was resistant to inhibition by two Smo antagonists, cyclopamine and SANT-1 (Figures 3D and S2F), demonstrating that the activity of this mutant protein was independent of Smo. Importantly, all the stable cell lines (which also contain endogenous Gli2) were able to produce equivalent levels of Gli1 when stimulated with SAG, showing that they did not differ in their intrinsic capacity to activate Hh targets (Figure 3C). Since the Flp-In lines also expressed endogenous Gli2, the *Gli1* induction in response to SAG (Figure 3C) could not be used to infer the Hh-responsiveness of the HA-Gli2 variants expressed in these lines.

To analyze the ability of upstream Hh signaling to regulate the HA-Gli2 mutants in our Flp-In cell lines, we selectively depleted endogenous Gli2 with a small interfering RNA (siRNA) directed against its 3' UTR (Figures 3E and S2G). Under these conditions,

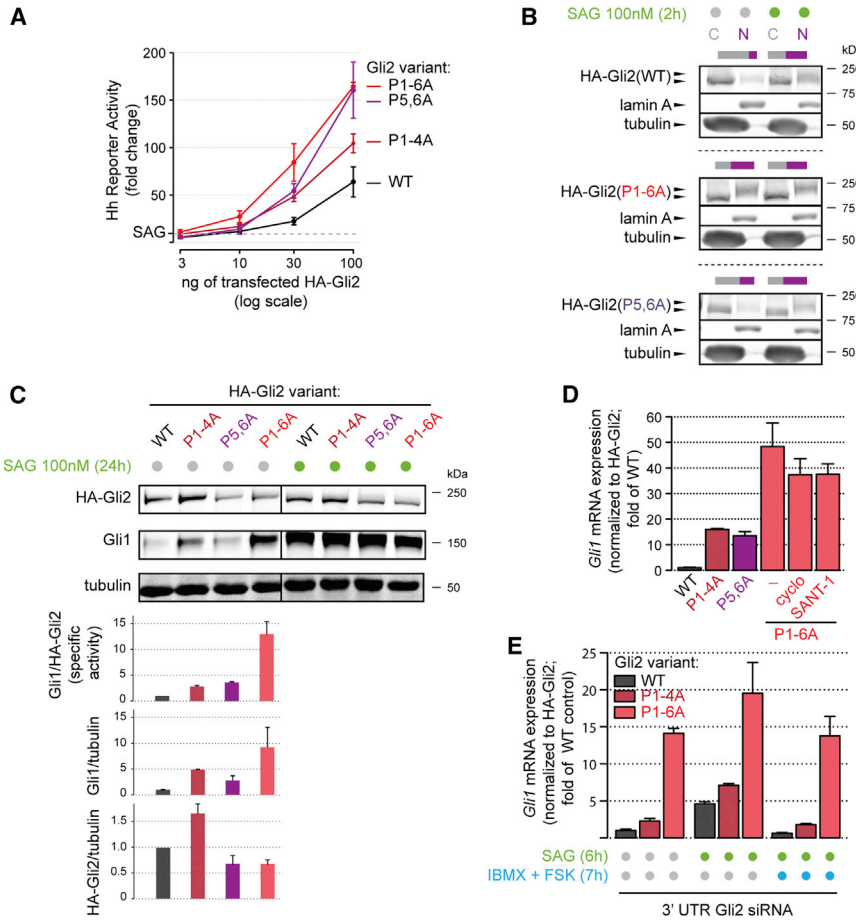


**Figure 3. The P1-6 Cluster Regulates the Activation of Gli2**

(A) Luciferase reporter activity in NIH/3T3 cells (untreated with any Hh agonists) transiently transfected with the indicated Gli2 variants. The dashed line shows levels of reporter induction seen when cells transfected with a control vector are exposed to SAG (100 nM). Error bars denote SD from three independent transfections.

(B) Distribution of full-length HA-Gli2 in NIH/3T3 Flp-In cells stably expressing the indicated variants.

(C) Levels of the Hh target gene *Gli1* and HA-Gli2, measured using anti-Gli1 and anti-HA immunoblots respectively, in NIH/3T3 Flp-In stable cell lines expressing the indicated Gli2 variants. Cells were left untreated or treated with SAG (100 nM, 24 hr). Bar charts underneath show quantitation of the *Gli1* and HA-Gli2 proteins (normalized to tubulin) in each cell line and the specific activity of each variant (top chart), expressed as the ratio of the intensities of the *Gli1* band to the HA band. Bars denote the mean ( $\pm$ SD) from two independent experiments.

(D) *Gli1* mRNA level, measured by quantitative RT-PCR, in Flp-In stable cell lines expressing the indicated HA-Gli2 variants. HA-Gli2(P1-6A) cells were left untreated or treated with the Smo inhibitors cycloamine (5  $\mu$ M) or SANT-1 (100 nM). The *Gli1* mRNA level was normalized to the HA-Gli2 protein level as in (C) to adjust for differences in expression level of the Gli variants. Bars denote the mean ( $\pm$ SD) from two independent samples.

(E) *Gli1* mRNA level in the indicated stable cell lines treated with SAG (100 nM) in the presence or absence of the PKA activators IBMX (100  $\mu$ M) and FSK (0.1  $\mu$ M). In all cells, expression of endogenous Gli2 was reduced by a siRNA directed

against the 3' UTR to examine signaling through the HA-Gli2 variants. The *Gli1* mRNA level was normalized to HA-Gli2 protein measured as in (C) and (D); graphs depicting data without the HA-Gli2 protein normalization are shown in Figures S2F and S2G. Bars denote the mean ( $\pm$ SD) from two independent samples.

the SAG initiated signal should be largely transduced through our HA-tagged Gli2 variants. In the absence of endogenous Gli2, SAG could significantly increase *Gli1* expression in either HA-Gli2(WT) or HA-Gli2(P1-4A) cells. In the same cell lines, PKA activation, accomplished with the drugs isobutylmethylxanthine (IBMX) and forskolin (FSK) antagonized the effect of SAG (Figure 3E). In contrast, the high baseline expression of *Gli1* in the HA-Gli2(P1-6A) line was largely insensitive to regulation by either SAG or IBMX/FSK (Figures 3E and S2G). This is further evidence that Gli2(P1-6A) corresponds to a maximally active form of Gli2, which cannot be regulated by either Smo or PKA. Gli2(P1-4A) remains SAG and PKA sensitive, perhaps through phosphoregulation at the P5 and P6 sites. We conclude that only after losing all phosphates at sites P1-6 does Gli2 become a bona fide GliA. These data explain why the previously studied Gli2(P1-4A) mutant of Gli2 failed to fully activate Hh responses during development (Pan et al., 2009).

### P1-6 Mutants of Gli2 Ectopically Specify Ventral Cell Types in the Developing Spinal Cord

Encouraged by these results, we tested the ability of Gli2(P1-6A) to drive Hh-regulated cell fate decisions in vivo in a cell-autono-

mous manner. In the ventral neural tube, Shh acts as a graded signal that specifies the dorsal-ventral pattern of progenitor subtypes (Figure 4A). This precise spatial patterning is established by a gradient of Gli activity (Bai et al., 2004; Lei et al., 2004; Stamatiki et al., 2005), making the neural tube an ideal place to test the activities of our Gli2(P1-4A) and Gli2(P1-6A) mutants. Using in ovo electroporation techniques, we expressed the Gli2 mutants under the control of a weak SV40 early promoter in one-half of the neural tube of Hamburger-Hamilton (HH) stage 10-12 chicken embryos and examined the expression of various progenitor markers 48 hr later. Ectopic expression of Gli2(WT) did not alter the spatial arrangement of neuronal progenitors (Figures 4B-4D, top row, and Figure S3C) and also did not induce expression of *PTCH1*, a direct Hh target gene (Figure 4E, top row).

In contrast, overexpression of Gli2(P1-6A) at any position along the dorsoventral axis led to the ectopic specification of ventral cells, identified by the ventral-most progenitor domain (pFP/p3) marker FOXA2 and the p3 marker NKX2.2, both of which depend on the highest levels of Hh/Gli signaling (Figure 4B, bottom row, and Figure S3C). Gli2(P1-6A) could also induce NKX6.1, which labels the pFP, p3, pMN, and p2 progenitor

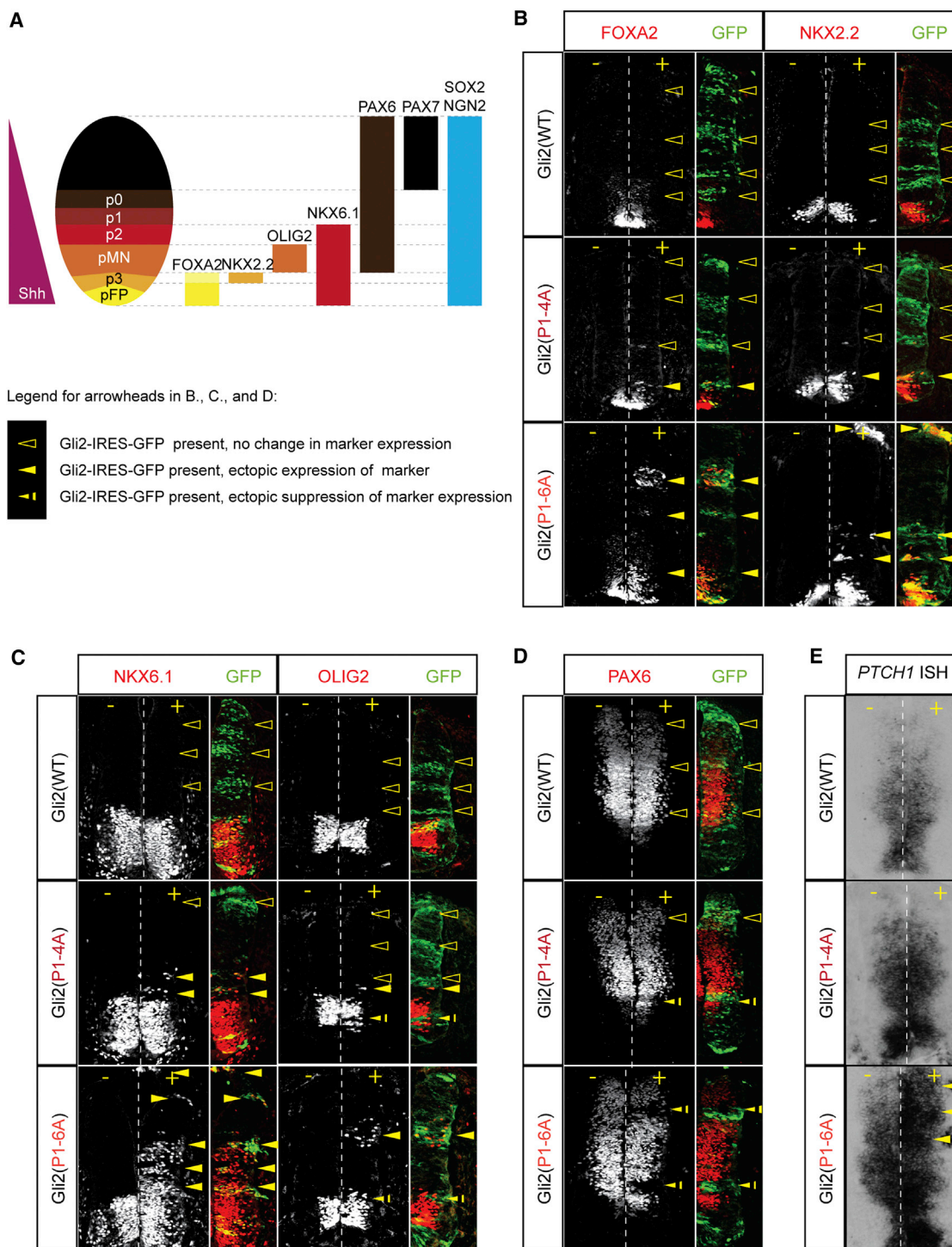
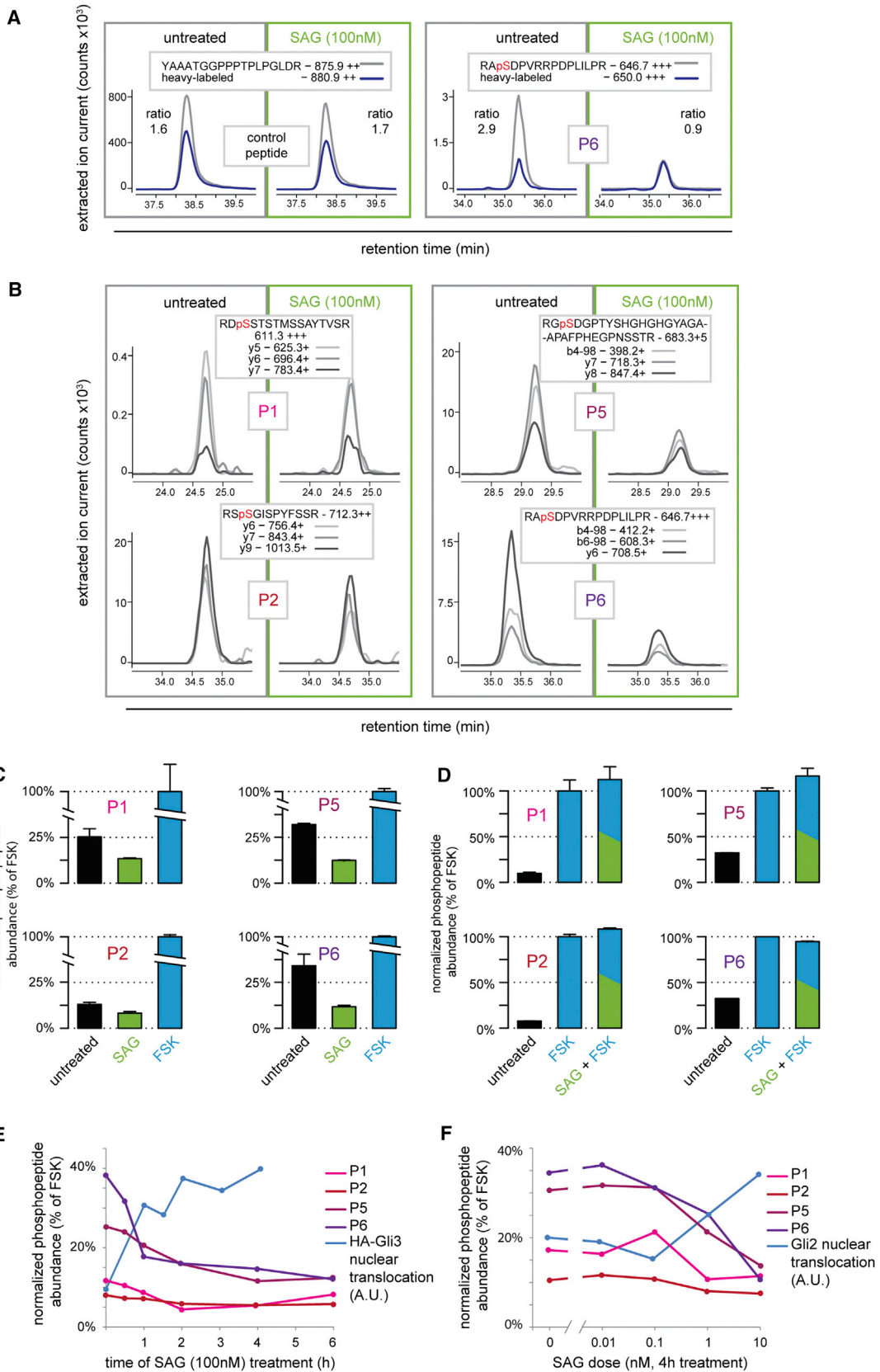


**Figure 4. Gli2(P1-6A) Can Induce Ventral Cell Fates in the Developing Spinal Cord**

(A) A schematic illustrating the relationship between marker proteins and progenitor cell populations in the embryonic neural tube (adapted from [Stamatakis et al., 2005](#)). pFP, floor plate progenitors; pMN, motor neuron progenitors; p0, p1, p2, p3, ventral interneuron progenitors.

(B–D) Constructs encoding Gli2 variants (green) were electroporated into developing spinal cords of chicken embryos. Expression of the indicated progenitor population markers (red) was detected by immunofluorescence 48 hr later. Black and white panels show marker expression in both sides of the spinal cord (“+” indicates the electroporated side, “–” the unelectroporated side). Overlay panels show the electroporated side only. See also [Figure S3C](#).

(E) In situ hybridization for *PTCH1* mRNA in sections of spinal cord electroporated with the indicated Gli2 constructs. The right side of each section was electroporated.



(legend on next page)

domains. OLIG2, a marker of motor neuron progenitors (pMN), which are specified by intermediate levels of Hh signaling, was induced mostly in cells expressing lower levels of Gli2(P1–6A) but often suppressed in strongly Gli2(P1–6A)-positive cells, most likely reflecting the cross-repressive interaction between NKX2.2 and OLIG2 in the neural tube (Novitsch et al., 2001). Moreover, Gli2(P1–6A) suppressed the expression PAX6, a dorsal marker known to be negatively regulated by Hh signaling. Consistent with this ability to specify cell fates that depend on high levels of Hh ligand, Gli2(P1–6A) induced the robust expression of *PTCH1*, a direct Hh target gene, throughout the neural tube. The ability Gli2(P1–6A) to induce the ventral and suppress the dorsal markers was resistant to coexpression of a constitutively active mutant of Patched, *Ptch<sup>Δloop2</sup>* (Briscoe et al., 2001), confirming that the P1–6A mutant of Gli2 escapes regulation by the upstream elements of the Hh pathway (Figure S3A).

Gli2(P1–4A) demonstrated intermediate activity: it induced FOXA2, NKX2.2, and NKX6.1 when expressed immediately adjacent to their normal domains but not when expressed in more dorsal regions of the neural tube (Figures 4B–4D, middle row, and Figure S3C). This expansion of the ventral domains suggests that Gli2(P1–4A) sensitized cells to Shh, such that the same level of Shh exposure is translated to more ventral cell fates. Even though our Gli2 variants induced ectopic FOXA2, they did not drive SHH expression (Figure S3B), suggesting that the effects we describe in Figure 4 were not due to non-cell-autonomous effects of ectopic floor plate induction in the electroporated spinal cords. These data are consistent with previous reports showing that activated Smo and Gli proteins expressed in the HH12 stage neural tube can promote ventral character while at the same time inhibiting the formation of floor-plate cells (Lei et al., 2004; Ribes et al., 2010). Neither Gli2 mutant affected the expression of Hh-independent progenitor markers SOX2 and NGN2, suggesting that the total number of neuronal progenitors is unchanged by the expression of these constructs (Figure S3B).

Taken together, these data suggest that there is a fundamental difference between blocking phosphorylation at sites P1–4 only and blocking it throughout the P1–6 cluster. Because both the P1–4A and P1–6A mutations block repressor formation (Figure 2B), the marked differences in the activities of Gli2(P1–4A) and Gli2(P1–6A), both in cultured cells and in the developing neural tube, must be attributed to the role of P5 and P6 in the

formation of Gli2A. Dephosphorylation of these sites in response to Hh ligands appears to be necessary to unleash the full activation potential of Gli2. P6 phosphorylation has been previously implicated in the interaction of Glis with 14-3-3 proteins (Asaoka et al., 2010), but in our system, this interaction did not appear to be required for the inhibitory function of P6 in GliA formation (see Supplemental Discussion and associated Figures S6B and S6C).

### Hh Signaling Reduces Phosphorylation of P1–6

Our mutagenesis studies suggested that loss of phosphorylation on the serine residues at P1–6 is a regulatory step in the activation of Gli proteins. Hence, we sought to monitor changes in the phosphorylation status of these sites on endogenous Gli2 in response to signaling. We were unable to raise phospho-specific antibodies that recognized multiple sites on endogenous Gli2 in a quantitative fashion. Instead, we developed a mass spectrometry (MS)-based selected reaction monitoring (SRM) assay to quantitatively assess phosphate occupancy at P1, P2, P5, and P6 (Cox et al., 2005; Gerber et al., 2003; Mayya et al., 2006). Endogenous Gli2, isolated by immunoaffinity purification, was digested with trypsin, and the phosphorylated versions of the tryptic peptides encompassing sites P1, P2, P5, and P6 were quantified by triple-quadrupole MS (Figure 5A).

Activation of Hh signaling by SAG reduced the abundance of phosphorylated peptides containing sites P1, P2, P5, and P6 (Figures 5B and 5C), with changes at P5 and P6 being more marked than those in sites P1 and P2. The phosphorylation of sites P5 and P6 was sensitive to both the concentration of SAG and the duration of SAG treatment (Figures 5E and 5F). In both cases, reduction in phosphorylation correlated with the amount of Gli in the nucleus. The changes in Gli2 phosphorylation were not due to differences in protein stability, since all measurements were conducted on cells pretreated with the proteasome inhibitor bortezomib and results obtained in the absence and presence of this drug were similar (Figures 5C and S4A). In addition, no changes were observed after SAG addition in the abundance of a control, nonphosphorylatable peptide from a different region of Gli2 (Figure 5A). A caveat with measuring dephosphorylation by quantitative MS is that the observed reduction in the abundance of a phosphopeptide might reflect a change in phosphate occupancy of nearby sites rather than actual dephosphorylation of the site of interest. To address this concern, we also monitored the nonphosphorylated

### Figure 5. Phosphorylation of the P1–6 Sites Declines with Hh Signaling

(A) Measurement of phosphopeptide abundance using SRM. Peptides were monitored in tryptic digests of immunoprecipitated Gli2 either in untreated NIH/3T3 Flip-In cells or in cells treated for 4 hr with 100 nM SAG, both in the presence of the proteasome inhibitor bortezomib (1  $\mu$ M). The intensity of the “strongest” transition for two peptides, a nonphosphorylatable peptide used as a loading control (left) and a phospho-P6-containing peptide (right), was plotted versus retention time (XIC, extracted ion current; gray trace). Blue traces are XICs of the corresponding heavy isotope-labeled standard peptide spiked into the tryptic digest before the run. For each condition, the normalized abundance of a peptide was calculated as the ratio of the area under the curve (AUC) for the light (endogenous) peptide to the AUC for the heavy peptide.

(B) XIC versus retention time plots showing three SRM transitions for each of the endogenous (light) phosphorylated peptides containing sites P1, P2, P5, and P6. (C and D) Normalized abundance of phosphopeptides (calculated using an SRM assays of the kind shown in A) containing the P1, P2, P5, and P6 sites derived from tryptic digests of immunopurified Gli2 isolated from NIH/3T3 cells treated (4 hr) with SAG (100 nM) or IBMX (100  $\mu$ M) + FSK (100 nM). Phosphopeptide abundance measured in cells after PKA activation with IBMX + FSK was taken as maximal (100%) phosphorylation. Bars denote means ( $\pm$ SD) of two to three independent MS runs.

(E and F) Phosphopeptide abundance was monitored as a function of time after SAG treatment (E) and as a function of SAG concentration (F) and compared to the levels of Gli3 (E) or Gli2 (F) in the nucleus (blue line). Percent of total Gli in the nucleus was calculated based on subcellular fractionation experiments as shown in Figure 2C (Humke et al., 2010).

peptide encompassing site P6 (dephospho-P6) by SRM and observed that its abundance rose with SAG treatment and declined with IBMX and FSK (reciprocal to the pattern seen with phospho-P6; [Figure S4B](#)), suggesting that the changes in phospho-P6 were due to bona fide dephosphorylation of the P6 site.

Stimulation of PKA activity with IBMX and FSK strongly increased phosphate occupancy at all sites within the P1–6 cluster and also prevented SAG from decreasing phosphorylation ([Figure 5D](#)). This result is consistent with the model that PKA negatively regulates Hh signaling by phosphorylating P1–6. It also suggests that even in resting cells, Gli proteins are not fully phosphorylated at the P1–6 sites. The reason why these partially dephosphorylated Glis do not become transcriptionally active is unknown but may be related to the dynamics of the phosphate turnover on individual sites within the cluster. For instance, there may be some redundancy between individual sites in the P1–4 and P5,6 clusters.

### A Cluster of Serine/Threonine Sites Is Important for Gli2/3 Activation

Since phosphorylation of the P1–6 cluster seemed sufficient for the inhibition of GliA formation, we were curious to determine how the two remaining clusters of putative PKA target sites (Pc–g, Pm–o; [Figures 1B and 1C](#)) affected Gli function. Alanine mutations in Pm–o cluster did not have a discernable effect ([Figure S5A](#)) in our assays, so we focused on the Pc–g cluster. To explore the role of Pc–g phosphorylation in the regulation of Gli2, we made both nonphosphorylatable and phosphomimetic mutations of this cluster in Gli2, replacing the serine and threonine residues with alanine or glutamate [hereafter called Gli2(Pc–gA) and Gli2(Pc–gE)]. In Hh reporter assays, HA-Gli2(Pc–gE) was significantly more active than the WT protein ([Figure 6A](#)) and Gli2(Pc–gA) was approximately 40% less active than the WT protein ([Figure 6B](#)). We also generated cell lines stably expressing HA-Gli2(Pc–gE) using the Flp-In system. Gli2(Pc–gE) protein levels were lower than Gli2 (WT), suggesting that the mutant protein was less stable ([Figure S5B](#)). The higher specific activity of HA-Gli2(Pc–gE) ([Figure 6C](#)) supported the model that Pc–g phosphorylation, in contrast to P1–6 phosphorylation, plays a positive role in Gli2 activity. Gli2(Pc–gE) also showed other hallmarks of activation, including reduced mobility on a gel and higher levels in the nucleus ([Figure 6D](#)).

### Hh Signaling Promotes and PKA Antagonizes Phosphorylation on Pg

The characterization of Pc–g phosphorylation as playing a positive role in Gli activity was inconsistent with our initial identification of these sites as *in vitro* targets for PKA ([Figure 1](#)), a kinase that has an inhibitory effect on Hh signaling in vertebrates ([Epstein et al., 1996](#); [Humke et al., 2010](#); [Tukachinsky et al., 2010](#); [Tuson et al., 2011](#)). To monitor Pc–g phosphorylation in the context of endogenous Gli2 in cells, we established an SRM assay to measure levels of a phosphorylated tryptic peptide that encompassed Pg, the only site in the Pc–g cluster whose phosphorylation could be easily monitored by MS ([Table S1](#)). Surprisingly, in cells treated with FSK and IBMX to activate PKA, Pg phosphorylation was reduced ([Figure 6E](#)), demon-

strating that the Pg site is not a bona fide PKA target in cells. Instead, we observed a 5-fold increase in the abundance of phosphorylated Pg upon SAG treatment ([Figure 6E](#)), supporting the mutational data pointing to a positive role for Pc–g phosphorylation in Gli2 activity. As for P6, we also monitored the abundance of a nonphosphorylated tryptic peptide encompassing site Pg (dephospho-Pg; [Figure S5C](#)). As expected, dephospho-Pg abundance dropped with SAG treatment and increased with IBMX + FSK treatment, providing further evidence for the positive regulation of Pc–g phosphorylation by the Shh signal. Experiments performed in the presence and absence of a proteasome inhibitor gave qualitatively similar results ([Figure S5D](#)).

Interestingly, both the temporal dynamics and SAG dose-sensitivity of Pc–g phosphorylation ([Figures 6F and 6G](#)) mirrored those of P1–6 dephosphorylation ([Figures 5E and 5F](#)). PKA activation had opposite effects on the phosphorylation of the Pc–g and P1–6 clusters, suppressing the former while promoting the latter ([Figures 6E and 5D](#)). A parsimonious interpretation of these data is that PKA prevents Pc–g phosphorylation and Gli activation by directly phosphorylating the P1–6 sites.

To dissect the hierarchy between the Pc–gE and P1–6 sites, we combined activating (Pc–gE) and inhibitory (Pc–gA) mutations in the Pc–g sites with either inactivating (P5,6D) or activating (P1–6A) mutations in the P1–6 sites ([Figure 6H](#)). In Hh reporter assays, the activities of the Gli2(Pc–gE/P5,6D) and Gli2(Pc–gE/P1–6A) combination mutants were very similar, demonstrating that activating modifications at Pc–g make the phosphorylation status of P1–6 irrelevant. Controls confirmed that the isolated P5,6D mutation is much less active than the P1–6A mutant. Conversely, introduction of the inactivating Pc–gA mutation into Gli2(P1–6A) caused a substantial drop in its constitutive activity both in transient transfection assays ([Figure 6I](#)) and in a stable cell line ([Figure 6J](#)). These results support the model that Pc–g phosphorylation is an activating event gated by PKA-regulated phosphorylation of the P1–6 sites.

## DISCUSSION

### Distinct Phospho-codes for Gli Activator and Gli Repressor Regulation

We show here that phosphorylation of Gli proteins at six PKA target sites (P1–6) is a central determinant of their transcriptional activity, controlling the production of both repressor (GliR) and activator (GliA) forms. Our data are most consistent with a model involving ordered changes of phosphate occupancy at sites located in two distinct serine/threonine clusters ([Figure 7A](#)). In resting cells, PKA phosphorylates sites P1–6 on Gli2/3, triggering proteasomal processing into GliR and blocking conversion into GliA. When Hh binds to Ptc, Smo inhibits P1–6 phosphorylation, initiating a pathway that ultimately leads to the production of GliA: Gli proteins undergo phosphorylation at the Pc–g cluster, enter the nucleus, and are converted to unstable transcriptional activator proteins. We propose that the full transcriptional activation of Gli proteins requires the loss of phosphates at the P1–6 cluster followed by the gain of phosphates at the Pc–g cluster. The relative ordering of these two events is demonstrated by the fact that PKA activation enhances P1–6 phosphorylation and blocks Pc–g phosphorylation

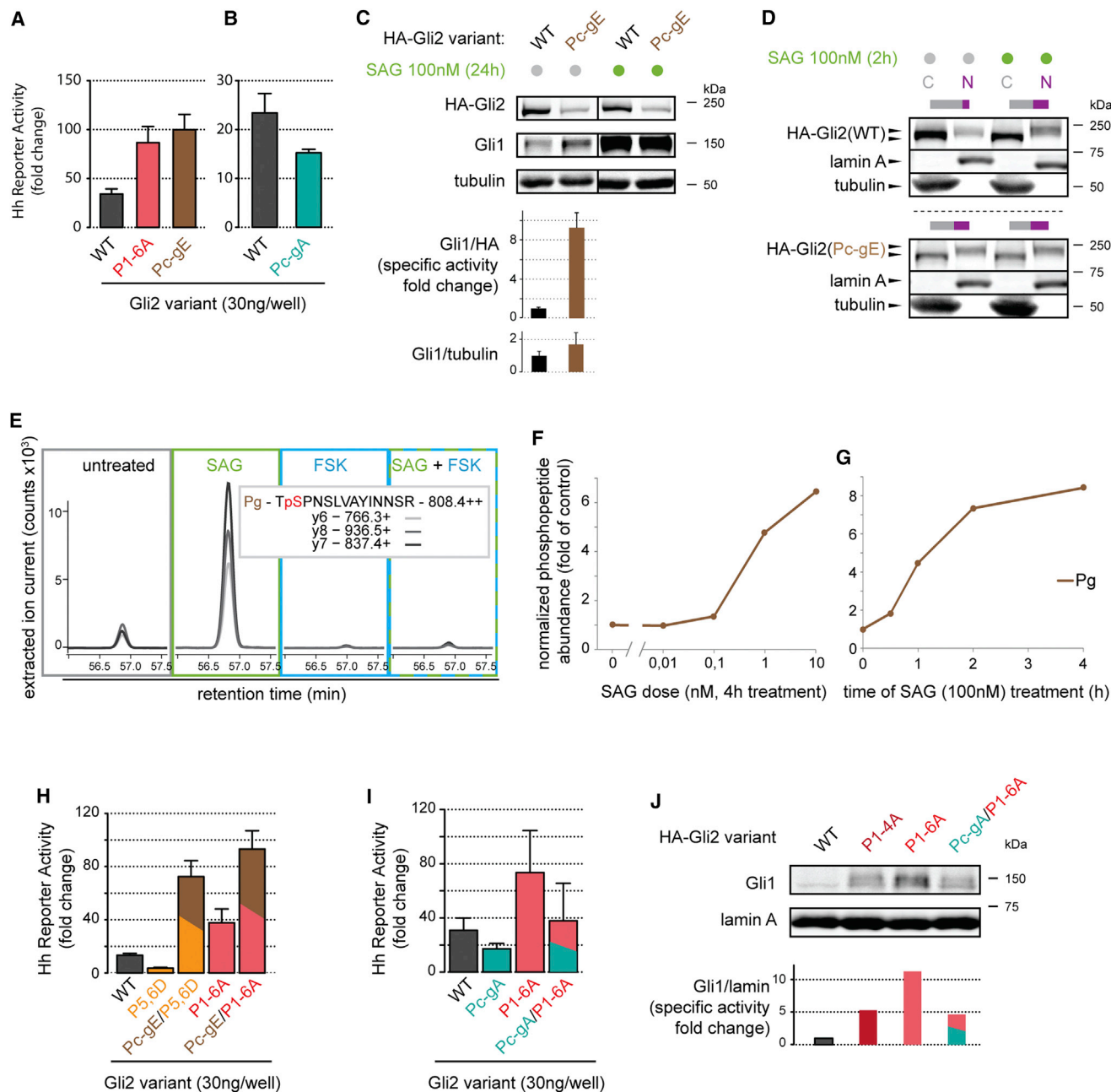


**Figure 6. Pc-g Phosphorylation Positively Regulates Gli2 Activity**

(A and B) Hh reporter activity in NIH/3T3 cells transiently transfected with Gli2(WT), Gli2(Pc-gA) or Gli2(Pc-gE). Bars are mean ( $\pm$ SD) of two independent transfections.

(C and D) NIH/3T3 Flp-In cell lines expressing HA-Gli2(WT) or HA-Gli2(Pc-gE) were used to evaluate the specific activity (C, analyzed as in Figure 3C) and subcellular distribution (D, analyzed as in Figure 2C) of the Gli2 variants. Bars are mean ( $\pm$ SD) of three independent experiments.

(E) XIC versus retention time traces for three SRM transitions derived from a Gli2 tryptic phosphopeptide containing the Pg residue. Phosphopeptide abundance is compared for Gli2 immunopurified from cells treated with the indicated drugs (4 hr).

(F and G) Pg phosphorylation abundance as a function of the concentration of SAG (F) or the duration of SAG exposure (G).

(H) Hh reporter activity in NIH/3T3 cells transiently transfected with Gli2(WT), Gli2(P5,6D), Gli2(P1-6A), and the combined mutants Gli2(Pc-gE/P1-6A) and Gli2(Pc-gE/P5,6D). Bars are mean ( $\pm$ SD) of three independent transfections.

(I) Hh reporter activity in NIH/3T3 cells transiently transfected with Gli2(WT), Gli2(Pc-gA), Gli2(P1-6A), and the combined mutant Gli2(Pc-gA/P1-6A). Bars denote mean  $\pm$  SD from two independent transfections.

(J) Level of the Hh target gene Gli1 measured using anti-Gli1 immunoblot in cell lines stably expressing near-endogenous levels of the indicated HA-Gli2 constructs. Bar chart shows quantitation of Gli1 protein normalized to lamin.

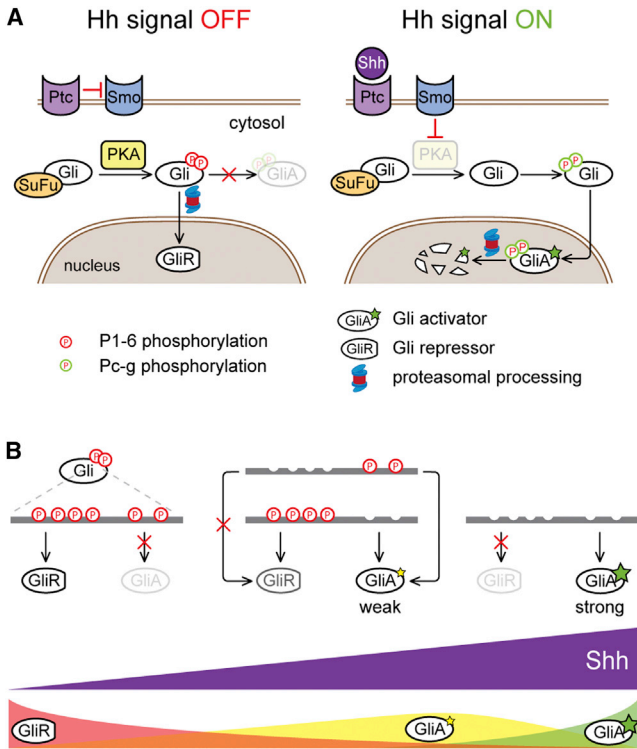


**Figure 7. Our Model for the Phosphoregulation of Gli Proteins in Hh Signaling**

(A) Diagram illustrating the multisite phosphorylation model of Gli2/3 regulation.

(B) Multiple states of Gli activity can be encoded by different patterns of Gli phosphorylation at the P1–6 cluster. Full phosphorylation of P1–6 (left) drives GliR formation and blocks GliA formation. Partially dephosphorylated Gli proteins (middle) function as weak activators and may be able to form GliR, depending on the pattern of phosphorylation. Fully dephosphorylated Gli proteins (right) cannot form GliR and function as strong transcriptional activators. See also [Supplemental Discussion](#).

(Figure 6E). This regulatory motif, a gating dephosphorylation event coupled to nuclear translocation and an activating phosphorylation event at a distinct site, is reminiscent of the mechanism by which nuclear factor of activated T cells (NFAT) is regulated in response to T cell receptor engagement (Okamura et al., 2000). The concerted dephosphorylation of 13 phosphoserine residues by the phosphatase calcineurin triggers a conformational change in NFAT that drives nuclear localization. Like the Gli proteins, NFAT also requires an activating phosphorylation event at a separate site to acquire full transcriptional activity. Interestingly, in Gli1, which acts as a strong constitutive activator, the P1–6 cluster is poorly conserved (only sites P1, P2, and P6 show some degree of conservation). By contrast, four out of the five sites in the Pc–g cluster, including Pg, show remarkable sequence conservation among the three mammalian Gli proteins. This suggests that Pc–g phosphorylation may act as a universal activating signal for the Gli family.

Many signaling pathways, such as the NFAT pathway, regulate the conversion of a transcription factor from an inactive to an active state. The Hh pathway is different in that it controls

the balance between gene repression, mediated by GliR, and gene activation, mediated by GliA. For instance, in *Drosophila*, low levels of Hh signaling suppress the formation of CiR, but higher levels are required for the production of CiA (Méthot and Basler, 1999, 2001). Our analysis of the P1–6 cluster in Gli3 (Figure 2) suggests that repressor and activator functions of Gli proteins can be encoded by different patterns of phosphorylation: loss of phosphates at P1–4 is enough to block repressor formation, but loss of phosphates at all six P1–6 residues is needed for full nuclear translocation and transcriptional activity (Figure 7B). This provides a simple mechanism by which signaling can exert independent control over the repressor and activator functions of Gli2/3.

While repressors forms of the Gli proteins can be assayed directly due to their truncated length, a reliable biochemical mark for Gli activator formation has remained elusive. GliA formation has been inferred indirectly from changes in subcellular localization, such as nuclear translocation, or from target gene activation. This is a clinically relevant issue, since such a mark of Gli protein activity would be a valuable predictive biomarker for patients being considered for Hh antagonists, and could be used as a pharmacodynamic parameter to assess responses. Our SRM MS analysis suggests that Pg phosphorylation can serve as such a marker for Gli2 activity.

### Graded Control of Gli Activity by Multisite Phosphorylation

Why might Gli proteins be regulated through such a complex phosphorylation scheme? Multisite phosphorylation is a commonly used regulatory module in diverse signaling systems (reviewed in Salazar and Höfer, 2009). It can be used to engineer an ultrasensitive ON/OFF switch or to encode a rheostat, allowing graded responses to varying signal strength. Examples of the latter include graded enhancement of p53 binding to CREB in response to genotoxic stress (Lee et al., 2010), graded binding of Ets-1 to DNA (Pufall et al., 2005), and graded regulation of the gating properties of the Kv2.1 potassium channel (Park et al., 2006). In fact, a theoretical model has shown that multisite phosphorylation may serve to refine such a rheostat by allowing multistability, the existence of multiple discrete activity states in the target protein or signaling module (Thomson and Gunawardena, 2009). A multistable rheostat would be well adapted to the function that Gli proteins serve during embryonic development. In developmental fields such as the limb, the inner ear, and the neural tube, Hh ligands function as classical morphogens, and a central task of signaling is to translate ligand exposure into discrete outputs, such as cell fate, at the level of transcription (Bai et al., 2004; Bok et al., 2007; Fuccillo et al., 2004; Stamatakis et al., 2005). Multisite phosphorylation might provide one mechanism by which differences in signal strength are converted into multiple discrete states of Gli activity (Figure 7B).

Indeed, our mutant analysis of the P1–6 cluster in Gli2 (Figures 3 and 4) is not consistent with a model in which Gli2 exists in either a fully inactive or fully active state. Particularly pertinent is the observation that both the P5,6A and the P1–4A mutants of Gli2 show an intermediate intrinsic capacity for transcriptional activation, which is higher than that of the WT protein but

significantly lower than that of the P1–6A mutant. Thus, Gli2 may occupy multiple states with differing activity, states that could represent different conformations of Gli2 that are stabilized by different patterns of phosphorylation at the P1–6 and Pc-g clusters. An important question going forward will be to ascertain how these changes in phosphate occupancy at the two conserved serine/threonine clusters affect the ability of Gli proteins to interact with other proteins in the cytoplasm, the cilium, and the nucleus and how these changes ultimately shape the Hh transcriptional program (also see [Supplemental Discussion](#)).

## EXPERIMENTAL PROCEDURES

### Cell Culture

293T cells, NIH/3T3 cells, and NIH/3T3 Flp-In cells (Life Technologies), including derivative stable clones, were cultured in media composed of Dulbecco's modified Eagle's medium (high glucose), 10% fetal bovine serum (FBS; Thermo Fisher Scientific), 1 × GlutaMAX, 1 × nonessential amino acids, 1 × sodium pyruvate, and 1 × penicillin/streptomycin (all from Life Technologies). Prior to harvesting, the cells were serum-starved in the same media but containing 0.5% FBS for 24–36 hr and treated with the indicated drugs/compounds. The 24 hr starvation was only used in assays where treatment time was 18–24 hr. For shorter treatment times (2–6 hr), a 36 hr starvation was preferred to induce a rapid response.

### In Vitro Phosphorylation

Myc-tagged Gli2/3 fragments were cloned into pCS2 and overexpressed in HEK293T cells. In vitro phosphorylation was carried out on immunoprecipitated proteins in the PKA reaction buffer (Promega) in the presence of 0.5 mM ATP, 10  $\mu$ Ci of [ $\gamma$ - $^{32}$ P]ATP, and 21 U of PKA (NEB) for 30 min at 30°C. See [Supplemental Experimental Procedures](#) for more details.

### Hedgehog Reporter Luciferase Assay

The Hedgehog reporter luciferase assay was performed as described by us before ([Dorn et al., 2012](#)). See [Supplemental Experimental Procedures](#) for more details. All plots are mean  $\pm$  SD.

### Generation of Stable Cell Lines

Stable cell lines expressing low levels of HA-tagged Gli2 and Gli3 variants were generated using the Flp-In method exactly according to the manufacturer's recommendations (Life Technologies). Briefly, cells were cotransfected with pOG44 and the pEF5/FRT/V5-DEST vector containing the Gli2/3 construct of interest. After 2 days, the cells were reseeded at low density and the culture media was supplemented with hygromycin for stable integrant selection. Stable cell lines were reselected with hygromycin on every other passage to preserve selection pressure and prevent silencing of the transgene.

### Subcellular Fractionation

The method for subcellular fractionation has been described by us in detail previously ([Humke et al., 2010](#)). Quantification of western blot bands was performed using ImageJ. Percent of the Gli2/3 variant present in the nuclear fractions was calculated for each sample by dividing the integrated band density for the nuclear fraction by the sum of densities for the cytoplasmic and nuclear fraction of the same sample.

### In Ovo Electroporation and Immunohistochemistry/In Situ Hybridization of Chick tissue

HH stage 10–12 chick embryos were electroporated as previously described ([Novitsch et al., 2001](#)) and incubated for  $\sim$ 48 hr to HH stages 20–22. See [Supplemental Experimental Procedures](#) for detailed methods of tissue staining and a list of reagents used.

### Selected Reaction Monitoring Mass Spectrometry

Cells from two to six confluent 150 mm tissue culture dishes were serum-starved for 36 hr and treated for indicated times with SAG and/or IBMX +

FSK. Bortezomib (1  $\mu$ M) was added 4 hr prior to harvesting unless indicated otherwise. The cell lysate was collected under denaturing conditions and then diluted in RIPA buffer for immunoprecipitation. Endogenous Gli2 was immunoprecipitated and the eluted protein was resolved using SDS-PAGE. The gel fragment containing Gli2 was excised and trypsinized. Tryptic fragments were extracted from the gel, purified using Oasis  $\mu$ Elution columns, and loaded onto a nano high-performance liquid chromatography system for separation and MS analysis ([Abell et al., 2011](#)). See [Supplemental Experimental Procedures](#) for more details regarding protein harvesting, purification, and SRM.

## SUPPLEMENTAL INFORMATION

Supplemental Information includes Supplemental Discussion, Supplemental Experimental Procedures, six figures, and one table and can be found with this article online at <http://dx.doi.org/10.1016/j.celrep.2013.12.003>.

## ACKNOWLEDGMENTS

We would like to thank Siggie Nachtergaele, Andres Lebensohn, and Ganesh Pusapati for critical reading of the manuscript, Casey Hughes for technical assistance, and James Briscoe for insightful discussions. This work was supported by NIH grants R21NS074091 and R00CA129174 (to R.R.), R01NS072804 and R01NS053976 (to B.G.N.), and P50GM107615 (to M.T.) and by grants from the V Foundation (to R.R.), the Sontag Foundation (to R.R.), the German Research Foundation (grant AH 220/1-1, to R.A.), and the March of Dimes Foundation (grant 6-FY10-296, to B.G.N.).

Received: September 30, 2013

Revised: November 7, 2013

Accepted: December 3, 2013

Published: December 26, 2013

## REFERENCES

- Abell, E., Ahrends, R., Bandara, S., Park, B.O., and Teruel, M.N. (2011). Parallel adaptive feedback enhances reliability of the Ca<sup>2+</sup> signaling system. *Proc. Natl. Acad. Sci. USA* *108*, 14485–14490.
- Asaoka, Y., Kanai, F., Ichimura, T., Tateishi, K., Tanaka, Y., Ohta, M., Seto, M., Tada, M., Ijichi, H., Ikenoue, T., et al. (2010). Identification of a suppressive mechanism for Hedgehog signaling through a novel interaction of Gli with 14-3-3. *J. Biol. Chem.* *285*, 4185–4194.
- Bai, C.B., Stephen, D., and Joyner, A.L. (2004). All mouse ventral spinal cord patterning by hedgehog is Gli dependent and involves an activator function of Gli3. *Dev. Cell* *6*, 103–115.
- Aza-Blanc, P., Ramirez-Weber, F.A., Laget, M.P., Schwartz, C., and Kornberg, T.B. (1997). Proteolysis that is inhibited by hedgehog targets Cubitus interruptus protein to the nucleus and converts it to a repressor. *Cell* *89*, 1043–1053.
- Bok, J., Dolson, D.K., Hill, P., R  ther, U., Epstein, D.J., and Wu, D.K. (2007). Opposing gradients of Gli repressor and activators mediate Shh signaling along the dorsoventral axis of the inner ear. *Development* *134*, 1713–1722.
- Briscoe, J., and Th  ron, P.P. (2013). The mechanisms of Hedgehog signaling and its roles in development and disease. *Nat. Rev. Mol. Cell Biol.* *14*, 416–429.
- Briscoe, J., Chen, Y., Jessell, T.M., and Struhl, G. (2001). A hedgehog-insensitive form of patched provides evidence for direct long-range morphogen activity of sonic hedgehog in the neural tube. *Mol. Cell* *7*, 1279–1291.
- Corbit, K.C., Aanstad, P., Singla, V., Norman, A.R., Stainier, D.Y.R., and Reiter, J.F. (2005). Vertebrate Smoothed functions at the primary cilium. *Nature* *437*, 1018–1021.
- Cox, D.M., Zhong, F., Du, M., Duchoslav, E., Sakuma, T., and McDermott, J.C. (2005). Multiple reaction monitoring as a method for identifying protein post-translational modifications. *J. Biomol. Tech.* *16*, 83–90.

- Dorn, K.V., Hughes, C.E., and Rohatgi, R. (2012). A Smoothened-Evc2 complex transduces the Hedgehog signal at primary cilia. *Dev. Cell* 23, 823–835.
- Epstein, D.J., Marti, E., Scott, M.P., and McMahon, A.P. (1996). Antagonizing cAMP-dependent protein kinase A in the dorsal CNS activates a conserved Sonic hedgehog signaling pathway. *Development* 122, 2885–2894.
- Fan, C.M., Porter, J.A., Chiang, C., Chang, D.T., Beachy, P.A., and Tessier-Lavigne, M. (1995). Long-range sclerotome induction by sonic hedgehog: direct role of the amino-terminal cleavage product and modulation by the cyclic AMP signaling pathway. *Cell* 81, 457–465.
- Fuccillo, M., Rallu, M., McMahon, A.P., and Fishell, G. (2004). Temporal requirement for hedgehog signaling in ventral telencephalic patterning. *Development* 131, 5031–5040.
- Gerber, S.A., Rush, J., Stemman, O., Kirschner, M.W., and Gygi, S.P. (2003). Absolute quantification of proteins and phosphoproteins from cell lysates by tandem MS. *Proc. Natl. Acad. Sci. USA* 100, 6940–6945.
- Hahn, H., Wicking, C., Zaphiropoulos, P.G., Gailani, M.R., Shanley, S., Chidambaram, A., Vorechovsky, I., Holmberg, E., Uden, A.B., Gillies, S., et al. (1996). Mutations of the human homolog of *Drosophila* patched in the nevus basal cell carcinoma syndrome. *Cell* 85, 841–851.
- Hammerschmidt, M., Bitgood, M.J., and McMahon, A.P. (1996). Protein kinase A is a common negative regulator of Hedgehog signaling in the vertebrate embryo. *Genes Dev.* 10, 647–658.
- Hill, P., Wang, B., and Rüther, U. (2007). The molecular basis of Pallister Hall associated polydactyly. *Hum. Mol. Genet.* 16, 2089–2096.
- Hui, C.-C., and Angers, S. (2011). Gli proteins in development and disease. *Annu. Rev. Cell Dev. Biol.* 27, 513–537.
- Humke, E.W., Dorn, K.V., Milenkovic, L., Scott, M.P., and Rohatgi, R. (2010). The output of Hedgehog signaling is controlled by the dynamic association between Suppressor of Fused and the Gli proteins. *Genes Dev.* 24, 670–682.
- Hynes, M., Porter, J.A., Chiang, C., Chang, D., Tessier-Lavigne, M., Beachy, P.A., and Rosenthal, A. (1995). Induction of midbrain dopaminergic neurons by Sonic hedgehog. *Neuron* 15, 35–44.
- Jiang, J., and Struhl, G. (1995). Protein kinase A and hedgehog signaling in *Drosophila* limb development. *Cell* 80, 563–572.
- Kang, S., Graham, J.M., Jr., Olney, A.H., and Biesecker, L.G. (1997). GLI3 frameshift mutations cause autosomal dominant Pallister-Hall syndrome. *Nat. Genet.* 15, 266–268.
- Kim, J., Kato, M., and Beachy, P.A. (2009). Gli2 trafficking links Hedgehog-dependent activation of Smoothed in the primary cilium to transcriptional activation in the nucleus. *Proc. Natl. Acad. Sci. USA* 106, 21666–21671.
- Lee, C.W., Ferreón, J.C., Ferreón, A.C.M., Arai, M., and Wright, P.E. (2010). Graded enhancement of p53 binding to CREB-binding protein (CBP) by multisite phosphorylation. *Proc. Natl. Acad. Sci. USA* 107, 19290–19295.
- Lei, Q., Zelman, A.K., Kuang, E., Li, S., and Matise, M.P. (2004). Transduction of graded Hedgehog signaling by a combination of Gli2 and Gli3 activator functions in the developing spinal cord. *Development* 131, 3593–3604.
- Lepage, T., Cohen, S.M., Diaz-Benjumea, F.J., and Parkhurst, S.M. (1995). Signal transduction by cAMP-dependent protein kinase A in *Drosophila* limb patterning. *Nature* 373, 711–715.
- Li, W., Ohlmeyer, J.T., Lane, M.E., and Kalderon, D. (1995). Function of protein kinase A in hedgehog signal transduction and *Drosophila* imaginal disc development. *Cell* 80, 553–562.
- Mayya, V., Rezual, K., Wu, L., Fong, M.B., and Han, D.K. (2006). Absolute quantification of multisite phosphorylation by selective reaction monitoring mass spectrometry: determination of inhibitory phosphorylation status of cyclin-dependent kinases. *Mol. Cell. Proteomics* 5, 1146–1157.
- Méthot, N., and Basler, K. (1999). Hedgehog controls limb development by regulating the activities of distinct transcriptional activator and repressor forms of Cubitus interruptus. *Cell* 96, 819–831.
- Méthot, N., and Basler, K. (2001). An absolute requirement for Cubitus interruptus in Hedgehog signaling. *Development* 128, 733–742.
- Niewiadomski, P., Zhujiang, A., Youssef, M., and Waschek, J.A. (2013). Interaction of PACAP with Sonic hedgehog reveals complex regulation of the hedgehog pathway by PKA. *Cell. Signal.* 25, 2222–2230.
- Novitsch, B.G., Chen, A.I., and Jessell, T.M. (2001). Coordinate regulation of motor neuron subtype identity and pan-neuronal properties by the bHLH repressor Olig2. *Neuron* 31, 773–789.
- Okamura, H., Aramburu, J., García-Rodríguez, C., Viola, J.P., Raghavan, A., Tahiliani, M., Zhang, X., Qin, J., Hogan, P.G., and Rao, A. (2000). Concerted dephosphorylation of the transcription factor NFAT1 induces a conformational switch that regulates transcriptional activity. *Mol. Cell* 6, 539–550.
- Pan, D., and Rubin, G.M. (1995). cAMP-dependent protein kinase and hedgehog act antagonistically in regulating decapentaplegic transcription in *Drosophila* imaginal discs. *Cell* 80, 543–552.
- Pan, Y., Bai, C.B., Joyner, A.L., and Wang, B. (2006). Sonic hedgehog signaling regulates Gli2 transcriptional activity by suppressing its processing and degradation. *Mol. Cell. Biol.* 26, 3365–3377.
- Pan, Y., Wang, C., and Wang, B. (2009). Phosphorylation of Gli2 by protein kinase A is required for Gli2 processing and degradation and the Sonic Hedgehog-regulated mouse development. *Dev. Biol.* 326, 177–189.
- Park, K.-S., Mohapatra, D.P., Misonou, H., and Trimmer, J.S. (2006). Graded regulation of the Kv2.1 potassium channel by variable phosphorylation. *Science* 313, 976–979.
- Price, M.A., and Kalderon, D. (1999). Proteolysis of cubitus interruptus in *Drosophila* requires phosphorylation by protein kinase A. *Development* 126, 4331–4339.
- Pufall, M.A., Lee, G.M., Nelson, M.L., Kang, H.-S., Velyvis, A., Kay, L.E., McIntosh, L.P., and Graves, B.J. (2005). Variable control of Ets-1 DNA binding by multiple phosphates in an unstructured region. *Science* 309, 142–145.
- Ribes, V., Balaskas, N., Sasai, N., Cruz, C., Dessaud, E., Cayuso, J., Tozer, S., Yang, L.L., Novitsch, B., Marti, E., and Briscoe, J. (2010). Distinct Sonic Hedgehog signaling dynamics specify floor plate and ventral neuronal progenitors in the vertebrate neural tube. *Genes Dev.* 24, 1186–1200.
- Riobó, N.A., Lu, K., Ai, X., Haines, G.M., and Emerson, C.P., Jr. (2006). Phosphoinositide 3-kinase and Akt are essential for Sonic Hedgehog signaling. *Proc. Natl. Acad. Sci. USA* 103, 4505–4510.
- Salazar, C., and Höfer, T. (2009). Multisite protein phosphorylation—from molecular mechanisms to kinetic models. *FEBS J.* 276, 3177–3198.
- Sasaki, H., Hui, C., Nakafuku, M., and Kondoh, H. (1997). A binding site for Gli proteins is essential for HNF-3beta floor plate enhancer activity in transgenics and can respond to Shh in vitro. *Development* 124, 1313–1322.
- Sasaki, H., Nishizaki, Y., Hui, C., Nakafuku, M., and Kondoh, H. (1999). Regulation of Gli2 and Gli3 activities by an amino-terminal repression domain: implication of Gli2 and Gli3 as primary mediators of Shh signaling. *Development* 126, 3915–3924.
- Stamatakis, D., Ulloa, F., Tsoni, S.V., Mynett, A., and Briscoe, J. (2005). A gradient of Gli activity mediates graded Sonic Hedgehog signaling in the neural tube. *Genes Dev.* 19, 626–641.
- Strutt, D.J., Wiersdorff, V., and Mlodzik, M. (1995). Regulation of furrow progression in the *Drosophila* eye by cAMP-dependent protein kinase A. *Nature* 373, 705–709.
- Tempé, D., Casas, M., Karaz, S., Blanchet-Tournier, M.-F., and Concordet, J.-P. (2006). Multisite protein kinase A and glycogen synthase kinase 3beta phosphorylation leads to Gli3 ubiquitination by SCFbetaTrCP. *Mol. Cell. Biol.* 26, 4316–4326.
- Thomson, M., and Gunawardena, J. (2009). Unlimited multistability in multisite phosphorylation systems. *Nature* 460, 274–277.
- Torres, J.Z., Miller, J.J., and Jackson, P.K. (2009). High-throughput generation of tagged stable cell lines for proteomic analysis. *Proteomics* 9, 2888–2891.
- Tukachinsky, H., Lopez, L.V., and Salic, A. (2010). A mechanism for vertebrate Hedgehog signaling: recruitment to cilia and dissociation of SuFu-Gli protein complexes. *J. Cell Biol.* 191, 415–428.

- Tuson, M., He, M., and Anderson, K.V. (2011). Protein kinase A acts at the basal body of the primary cilium to prevent Gli2 activation and ventralization of the mouse neural tube. *Development* 138, 4921–4930.
- Wang, B., and Li, Y. (2006). Evidence for the direct involvement of betaTrCP in Gli3 protein processing. *Proc. Natl. Acad. Sci. USA* 103, 33–38.
- Wang, G., Wang, B., and Jiang, J. (1999). Protein kinase A antagonizes Hedgehog signaling by regulating both the activator and repressor forms of Cubitus interruptus. *Genes Dev.* 13, 2828–2837.
- Wang, B., Fallon, J.F., and Beachy, P.A. (2000). Hedgehog-regulated processing of Gli3 produces an anterior/posterior repressor gradient in the developing vertebrate limb. *Cell* 100, 423–434.
- Wen, X., Lai, C.K., Evangelista, M., Hongo, J.-A., de Sauvage, F.J., and Scales, S.J. (2010). Kinetics of hedgehog-dependent full-length Gli3 accumulation in primary cilia and subsequent degradation. *Mol. Cell. Biol.* 30, 1910–1922.
- Zhou, C., Jacobsen, F.W., Cai, L., Chen, Q., and Shen, W.D. (2010). Development of a novel mammalian cell surface antibody display platform. *MAbs* 2, 508–518.

**Supplemental Information**

**Gli protein activity is controlled by multi-site phosphorylation  
in vertebrate Hedgehog signaling**

Pawel Niewiadowski, Jennifer H. Kong, Robert Ahrends, Yan Ma, Eric W. Humke, Sohini Khan,  
Mary N. Teruel, Bennett G. Novitch, and Rajat Rohatgi

**A**

R	R	X	S		full consensus PKA target site ( <b>P1-6</b> )
K	K	X	T		

R	X	X	S		partial consensus PKA target site (Pa-o)
K	X	X	T		

**B**

	Gli2	Gli3
<b>P1</b>	S789	S849
<b>P2</b>	S805	S865
<b>P3</b>	S817	S877
<b>P4</b>	S848	S907
<b>P5</b>	S923	S980
<b>P6</b>	S956	S1006

	Gli2	Gli3
<b>Pa</b>	S100	S177
<b>Pb</b>	S145	S223
<b>Pc</b>	S216	S281
<b>Pd</b>	T220	S285
<b>Pe</b>	S224	S289
<b>Pf</b>	S230	S295
<b>Pg</b>	S248	S313
<b>Ph</b>	S263	S338
<b>Pi</b>	S355	S419
<b>Pj</b>	S372	S435
<b>Pk</b>	S894	S952
<b>Pl</b>	S975	S1026
<b>Pm</b>	T1503	T1542
<b>Pn</b>	T1504	T1543
<b>Po</b>	S1508	S1547

**Figure S1, Related to Figure 1.**

(A) Sequences of full consensus and partial consensus PKA target sites.

(B) Residue numbers of conserved partial (orange) and full (red) consensus PKA target sites in mouse Gli2 and Gli3.

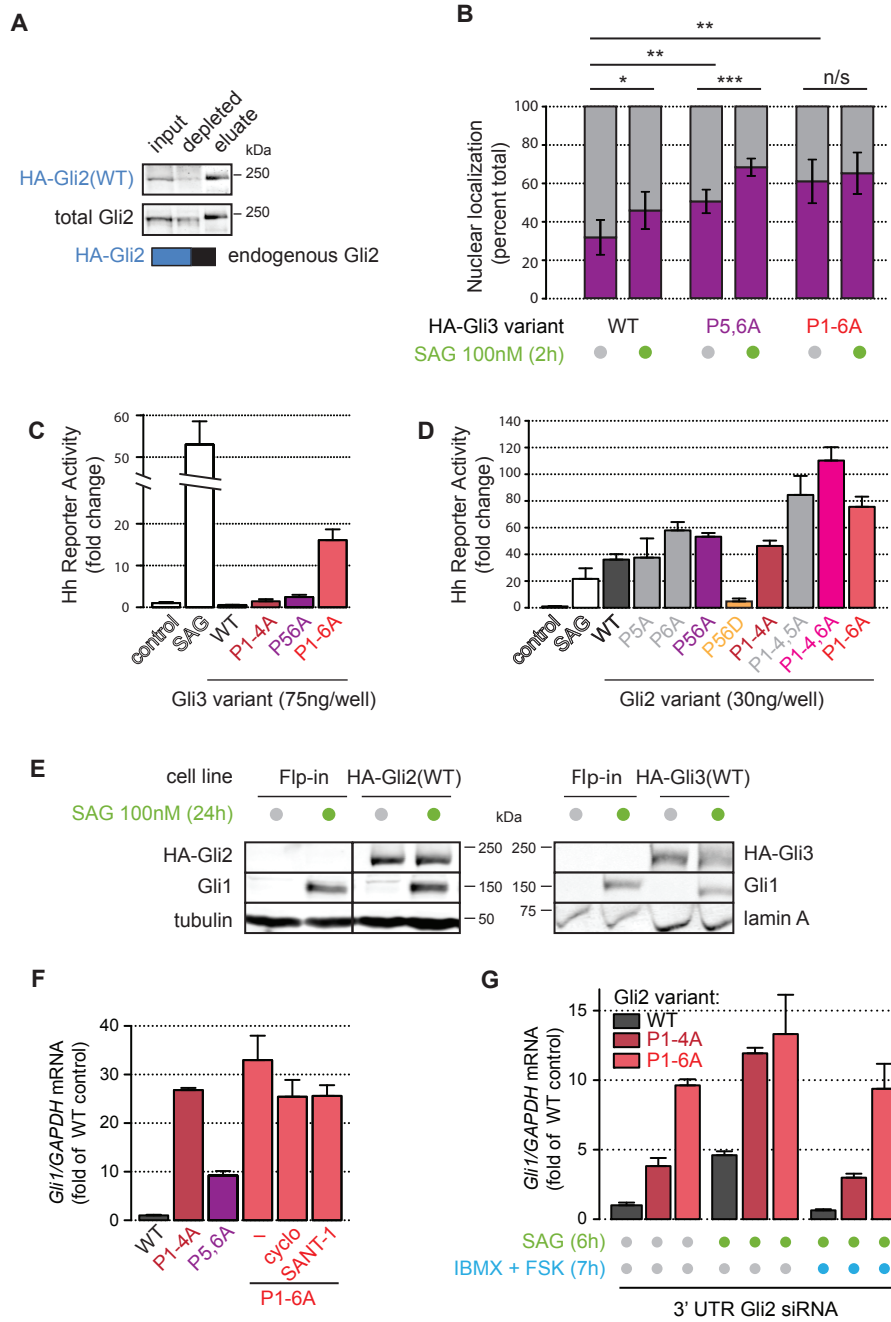


**Figure S2, Related to Figures 2 and 3.**

(A) Analysis of the levels of HA-tagged exogenous Gli2 compared to endogenous Gli2. Lysates from cells expressing wild-type HA-Gli2 were immunoprecipitated with anti-HA beads. Shown are anti-HA and anti-Gli2 immunoblots of the input (before immunoprecipitation) and the immunodepleted flow-through (after removal of the anti-HA beads). The beads deplete over 78% of HA-Gli2, while the total Gli2 (exogenous + endogenous) is depleted by 43%. The bar represents the calculated amount of exogenous and endogenous Gli2 as a fraction of the total cellular Gli2

(B) Statistical analysis of nuclear translocation data for HA-Gli3 variants. The nuclear/cytoplasmic fractionation was performed as in Figure 2C. Means  $\pm$  SD of percentage nuclear HA-Gli3 from  $n=5$  independent experiments are shown (purple bars); \* -  $p < 0.05$ , \*\* -  $p < 0.01$ , \*\*\* -  $p < 0.001$ , n/s – not significant

(C) Luciferase reporter activity in NIH/3T3 cells transiently transfected with the indicated Gli3 variants.

(D) Luciferase reporter activity in NIH/3T3 cells transiently transfected with the indicated Gli2 variants. In (C) and (D) error bars depict SD from 2-3 independent transfections.

(E) Levels of Gli1 and HA-Gli2, measured using anti-Gli1 and anti-HA immunoblots respectively, in NIH/3T3 Flp-In stable cell lines expressing HA-Gli2, HA-Gli3, or neither. Cells were left untreated or treated with SAG (100nM, 24h).

(F) *Gli1* mRNA level, measured by qRT-PCR, in Flp-In stable cell lines expressing the indicated HA-Gli2 variants. Samples are the same as in Figure 3D, but the *Gli1* mRNA level was normalized to the *GAPDH* housekeeping gene rather than to HA-Gli2 protein. Bars denote the mean ( $\pm$  SD) from 2 independent samples.

(G) *Gli1* mRNA level in the indicated stable cell lines transfected with Gli2 3'UTR siRNA and treated with SAG (100nM) in the presence or absence of the PKA activators IBMX (100 $\mu$ M) and FSK (0.1 $\mu$ M). Samples are the same as in Figure 3E, but the *Gli1* mRNA level was normalized to the *GAPDH* housekeeping gene rather than to HA-Gli2 protein. Bars denote the mean ( $\pm$  SD) from 2 independent samples.

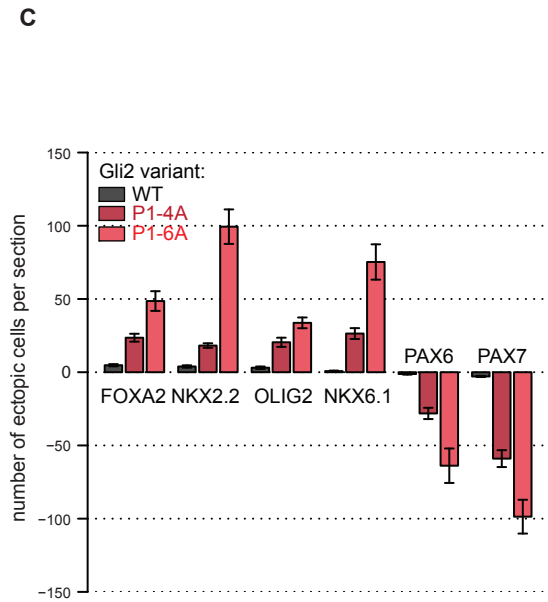
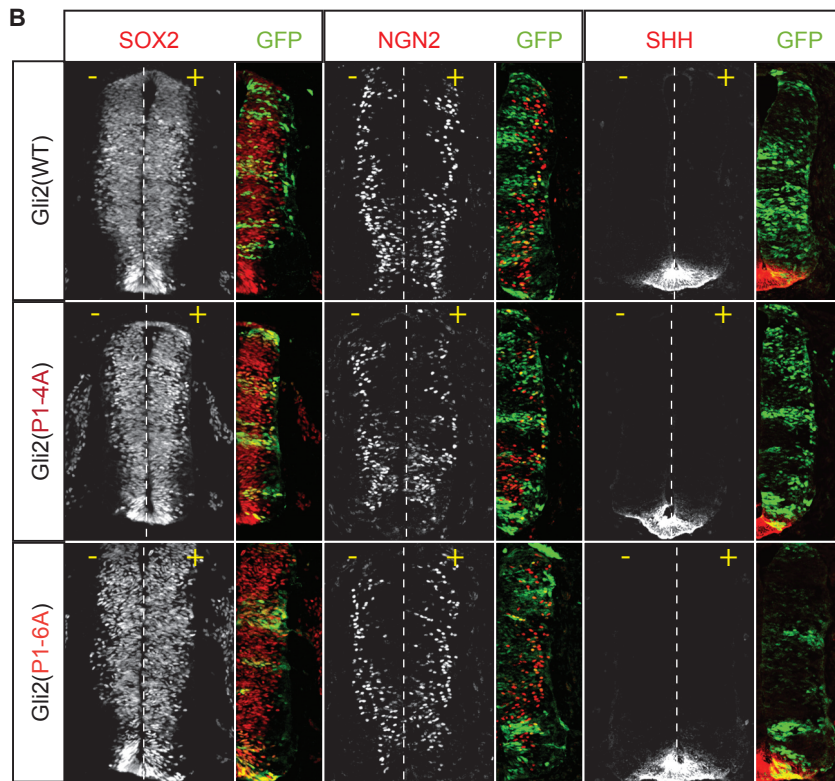
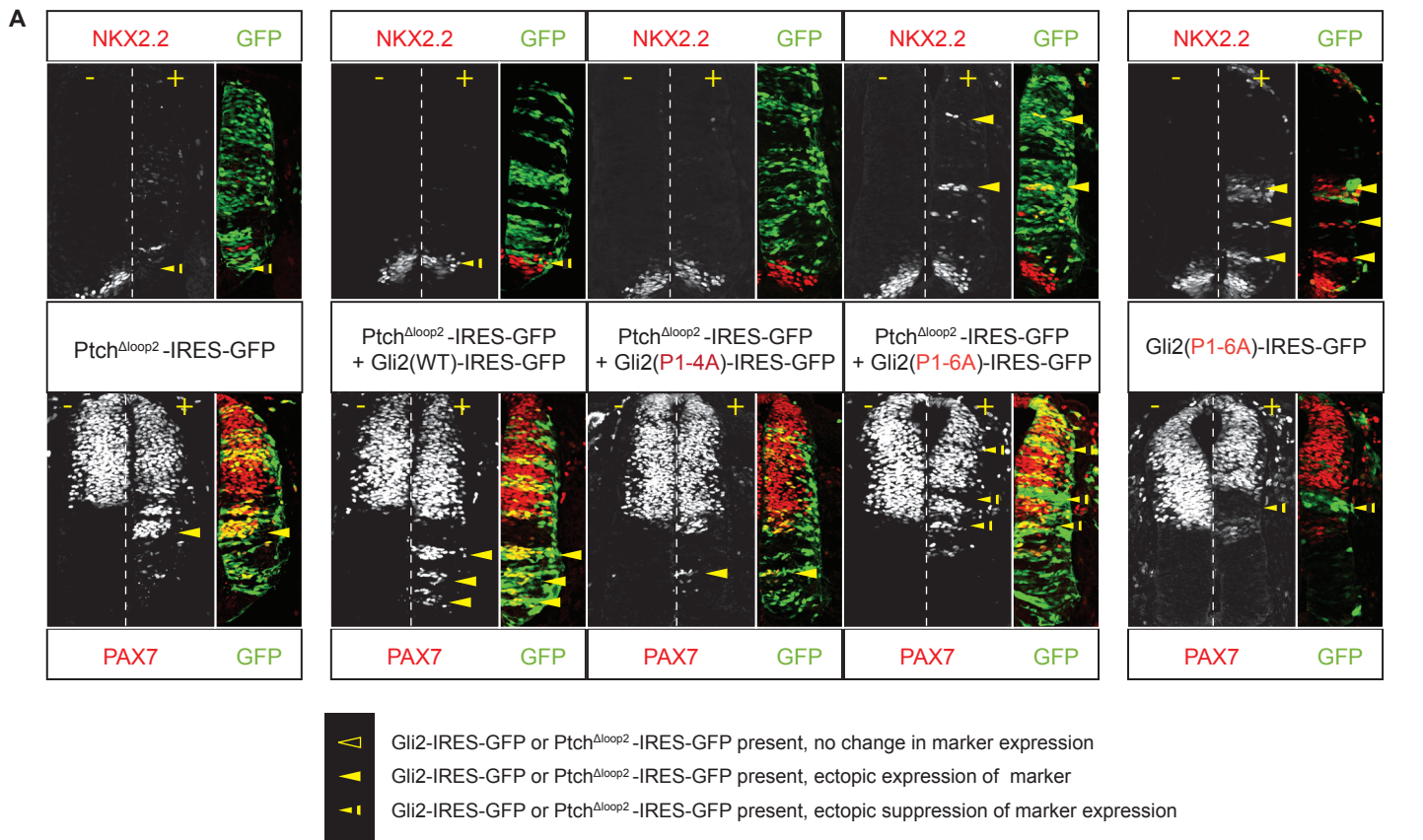


**Figure S3, Related to Figure 4.**

(A) Expression of ventral (NKX2.2) and dorsal (PAX7) markers (both in red) in chick spinal cord co-electroporated with the indicated Gli2 constructs (green) and the constitutively active variant of Patched - Ptch<sup>Δloop2</sup> (also green). Tissue was processed as in Figure 4.

(B) SOX2, NGN2, and SHH expression in chick spinal cord electroporated with the indicated Gli2 constructs. Experiment was performed as in Figure 4.

(C) Statistical analysis of the ectopic expression of neural progenitor markers in chick spinal cords electroporated with the indicated Gli2 constructs. Bars denote mean  $\pm$  SEM of GFP-positive ectopic progenitors per section from n=19-32 tissue sections. Negative numbers indicate suppression of progenitor markers within their normal expression domain.

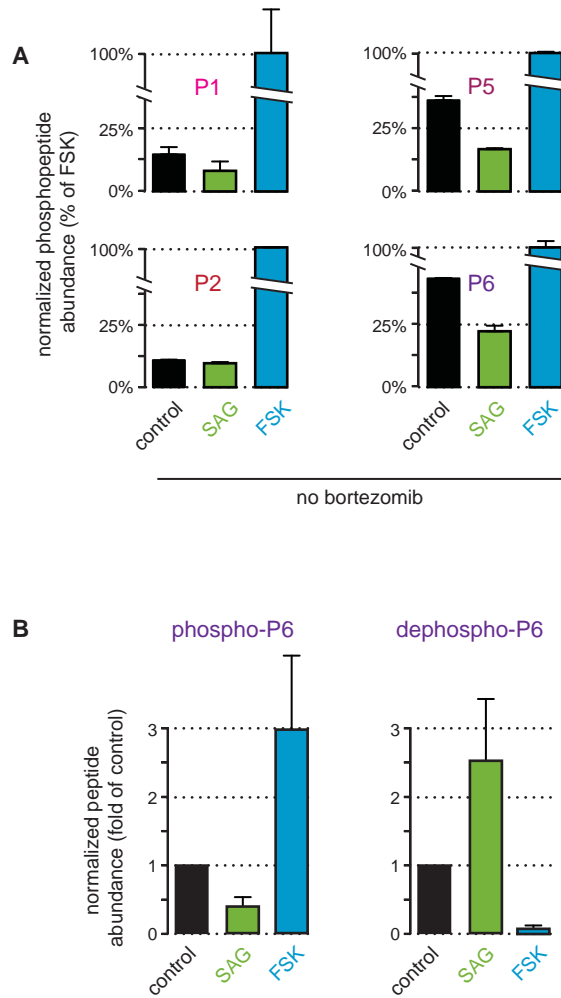


**Figure S4, Related to Figure 5.**

(A) Normalized phosphopeptide abundance in tryptic digests of Gli2 isolated from NIH/3T3 cells treated with or without SAG or IBMX+FSK in the absence of bortezomib. The experiment was performed as in Figure 5C. Error bars are SD from 2 independent MS runs.

(B) Normalized peptide abundance in tryptic digests of Gli2 isolated from NIH/3T3 cells treated with or without SAG or IBMX+FSK in the presence of bortezomib. The experiment was performed as in Figure 5C. Error bars are SD from 2-3 independent MS runs.

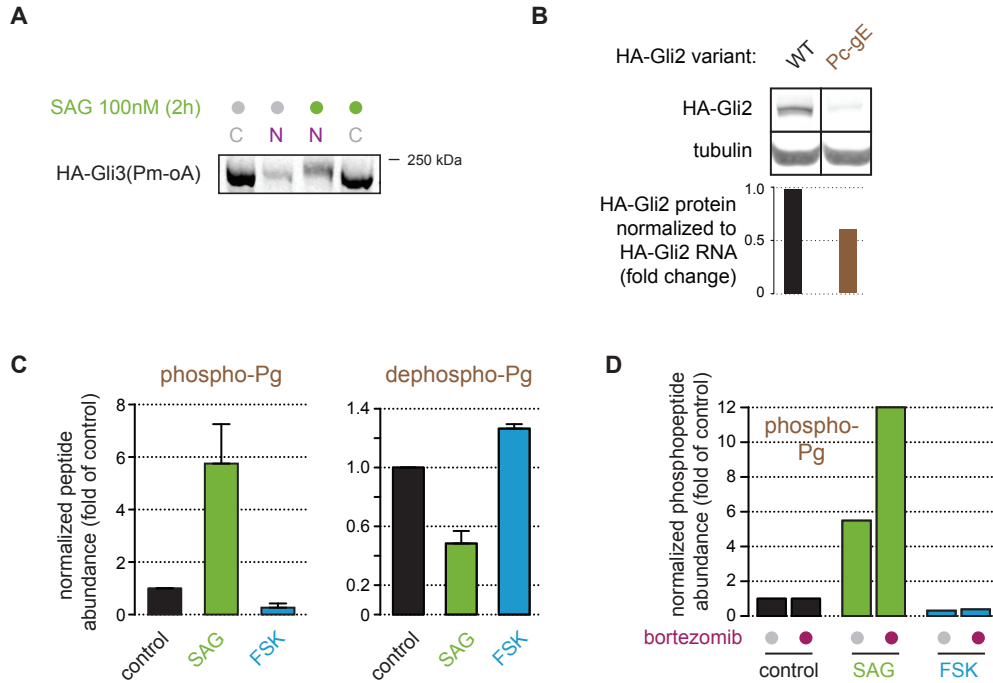


**Figure S5, Related to Figure 6.**

(A) Distribution of full-length HA-Gli3(Pm-oA) in the nuclear (N) and cytoplasmic (C) fractions of the NIH/3T3 Flp-In stable cell line left untreated or treated with SAG (100nM, 2h). The experiment was performed as in Figure 2C.

(B) Protein levels of HA-Gli2(WT) and HA-Gli2(Pc-gE) were measured in stable NIH/3T3 Flp-in lines by anti-HA immunoblot and mRNA levels were measured by quantitative RT-PCR. Bars represent protein expression levels normalized to mRNA levels.

(C) Normalized peptide abundance in tryptic digests of Gli2 isolated from NIH/3T3 cells treated with or without SAG or IBMX+FSK in the presence of bortezomib. The experiment was performed as in Figure 6E. Bars denote mean (+/- SD) from 2 independent MS runs.

(D) Normalized phosphopeptide abundance in tryptic digests of Gli2 isolated from NIH/3T3 cells treated with or without SAG or IBMX+FSK in the presence or absence of bortezomib. The experiment was performed as in Figure 6E.

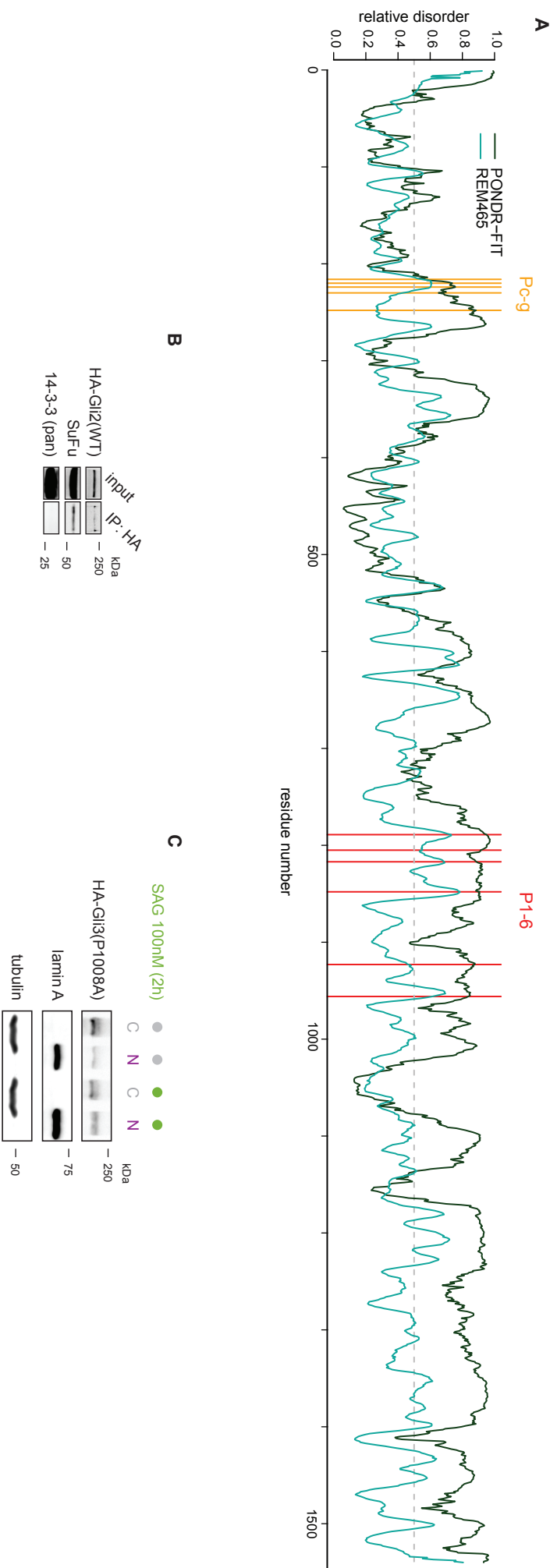


**Figure S6, Related to Supplemental Discussion.**

(A) Clusters of phosphorylated sites in Gli2 are located in regions of high disorder. Intrinsic disorder of the mouse Gli2 sequence was calculated using two algorithms: POND-R-FIT (Xue et al., 2010) and REM465 (Linding et al., 2003). Plots show relative disorder values of regions of Gli2 centered on the indicated residue number. Values higher than 0.5 indicate protein regions that are most likely unstructured. Positions of the phosphosites belonging to the P-c-g and P1-6 clusters are indicated by vertical lines.

(B) Immunoblots showing the amount of endogenous SuFu and 14-3-3 co-immunoprecipitated with HA-Gli2 from lysates of a stable NIH/3T3 Fip-in cell line.

(C) Levels of HA-Gli3(P1008A) in the cytoplasm and nucleus of untreated cells or cells treated for 2h with 100nM SAG. The P1008A mutant of Gli3 lacks the consensus proline site required for its putative interaction with 14-3-3. The experiment was performed using a stable NIH/3T3 Fip-in line as in Figure 2C.

Phospho-site	Peptide sequence	Precursor neutral mass	Heavy precursor neutral mass	Precursor charge	Fragment ion	Fragment neutral mass	Heavy fragment neutral mass	Fragment charge
Control	AHTGGTLDDGIR	1211.6	1221.6	2	y9	902.4	912.5	1
					y8	845.4	855.4	1
					y5	574.3	584.3	1
Control	YAAATGGPPPPTPLPGLDR	1749.9	1759.9	2	y11	1158.6	1168.6	1
					y10	1061.6	1071.6	1
					y7	766.4	776.4	1
P1	RDSS[+80]TSTM[+16]SSA YTVSR	1830.7	1840.8	3	y7	782.4	792.4	1
					y6	695.4	705.4	1
					y5	624.3	634.3	1
P2	RSS[+80]GISPYFSSR	1422.6	1432.6	2	y9	1012.5	1022.5	1
					y7	842.4	852.4	1
					y6	755.4	765.4	1
P5	RGS[+80]DGPTYSHGHG HGYAGAAPAFPHEGPNS STR	3411.5	3421.5	5	y8	846.4	856.4	1
					y7	717.3	727.3	1
					b4 - 98	397.2	397.2	1
P6	RAS[+80]DPVRRPDPLILP R	1937.0	1947.0	3	y8	919.5	929.6	1
					y6	707.5	717.5	1
					b4 - 98	411.2	411.2	1
					b6 - 98	607.3	607.3	1
dephospho-P6	ASDPVR	643,3	653,3	2	y5	572.3	582.3	1
					y4	485.3	495.3	1
					y3	370.2	380.2	1
Pg	TS[+80]PNSLVAYINNSR	1614.7	1624.7	2	y8	935.5	945.5	1
					y7	836.4	846.4	1
					y6	765.4	775.4	1
dephospho-Pg	TSPNSLVAYINNSR	1534.8	1544.8	2	y8	935.5	945.5	1
					y7	836.4	846.4	1
					y6	765.4	775.4	1

**Table S1, Related to Supplemental Experimental Procedures.**

Peptides and transitions monitored in the Selected Reaction Monitoring experiments.

## **SUPPLEMENTAL DISCUSSION**

### **Role of protein disorder in phospho-regulation of Gli proteins**

Gli proteins are predicted to be disordered in segments that overlap the Pc-g and P1-6 phosphosites (Figure S6A). Like for many other intrinsically unstructured proteins, multi-site phosphorylation of Glis might therefore control their conformation by affecting the order/disorder balance in these regions (Gsponer et al., 2008).

### **Regulation of Gli proteins by phosphorylation in the morphogen gradient**

Interestingly, recently published data on the role of GliA and GliR in ventral spinal cord development seem to support the notion of multiple discrete activation states of GliA (Oosterveen et al., 2012). In this paper, GliA was found to perform two distinct functions. In areas exposed to the highest concentrations of Hh, GliA was self-sufficient in specifying ventral-most progenitor cells. By contrast, in regions receiving intermediate to low concentrations of the morphogen, GliA was only permissive and instead GliR played the key role in cell fate determination. In view of our data, one plausible explanation is that fully dephosphorylated “strong” GliA proteins determine the boundaries of the ventral-most pFP and p3 regions, whereas partially dephosphorylated “weak” GliA proteins, most prevalent in the intermediate pMN-p0 regions, are non-instructive and subordinate to GliR in transducing the long-range Hh signal. The GliR gradient, critical for setting progenitor region boundaries in intermediate to dorsal areas of the neural tube, arises stochastically from the increasing probability of sites P1-4 being phosphorylated as the concentration of Hh goes down (Figure 7B).

### **Smo controls P1-6 phosphorylation**

In accordance with the notion that P1-6 phosphorylation stoichiometry regulates the GliR/GliA balance, we find that these sites undergo dephosphorylation when Smo is activated by its direct agonist SAG (Figure 5). There is some evidence that Smo can act as a G-protein coupled receptor (GPCR), activating  $G_{\alpha i}$ , reducing cyclic AMP (cAMP) levels, and reducing PKA activity (Chinchilla et al., 2010; Ogden et al., 2008; Polizio et al., 2011; Riobo et al., 2006; Shen

et al., 2013). However, some studies have suggested that  $G_{ci}$  is not absolutely required for canonical Hh signaling (Low et al., 2008; Polizio et al., 2011). An alternate mechanism has been suggested by the recent discovery that the inhibition of a ciliary  $G_{\alpha s}$ -coupled receptor Gpr161 by Smo is required for Hh signal transduction (Mukhopadhyay et al., 2013). It is tempting to speculate that Gpr161 maintains high baseline phosphorylation of Gli proteins by locally boosting cAMP levels and increasing PKA activity at primary cilia (Barzi et al., 2010, Niewiadomski et al., 2013) and that Smo promotes Gli dephosphorylation by antagonizing Gpr161.

### **Mechanism of Gli activation downstream of P1-6 dephosphorylation**

Our data suggests that loss of phosphorylation of the P1-6 cluster on Gli2/3 is a critical outcome of Smo activation. However, our mechanistic understanding of how the phosphorylation pattern is interpreted at the level of gene expression remains rudimentary. The most straightforward possibility is that phosphorylation simply influences the nucleocytoplasmic transport of Gli proteins, thereby regulating their availability at target promoters. In fact, the Gli nuclear localization sequence (NLS) within the fifth zinc finger domain is located adjacent to a conserved PKA target site and this site has been shown to affect Gli1 nuclear translocation (Sheng et al., 2006). However, our data suggest that sites P1-6, and not the one located near the NLS, play a decisive role in regulating Gli nuclear entry (Figures 2C and 3B). Since no predicted NLS has been described near the phosphosites in the P1-6 cluster, an alternate mechanism, perhaps based on conformational changes, must explain the effect of P1-6 phosphorylation on Gli nuclear accumulation.

Control of the nuclear concentration of Gli proteins may not be the only mechanism by which P1-6 phosphorylation influences the expression of Hh target genes. A prior study proposed that P6 phosphorylation induces the association of Gli proteins with 14-3-3 $\epsilon$ , which restricts their transcriptional activity in resting cells without affecting their nuclear localization (Asaoka et al., 2010). In our hands, however, 14-3-3 failed to associate with Gli2 even in when

the signal was off (Figure S6B), and a Gli3 mutant lacking a proline residue essential for 14-3-3 binding did not show signs of constitutive activation (Figure S6C). Thus, 14-3-3 binding does not appear to play a role in limiting GliA under the conditions used in our study.

Other than directly regulating nuclear trafficking and activity at target promoters, dephosphorylation of P1-6 may act by priming Gli proteins for additional posttranslational modifications (PTMs). Specifically, phosphorylation of the Pc-g cluster appears to occur downstream of the loss of phosphates at the P1-6 sites, and to be an important component of GliA formation. In addition to phosphorylation, Gli proteins have been shown to undergo ubiquitination (Di Marcotullio et al., 2007), acetylation (Canettieri et al., 2010) and SUMOylation (Cox et al., 2010), all of which alter their transcriptional potential. How these PTMs are integrated to allow Hh signaling to control gene expression in a graded fashion during morphogenesis is an important question for future studies to explore.

## SUPPLEMENTAL EXPERIMENTAL PROCEDURES

### Molecular cloning and site-directed mutagenesis

For the purpose of *in vitro* phosphorylation, short fragments of Gli2 and Gli3 were generated from full length mouse Gli2 and Gli3 clones by PCR. They were inserted into a custom pCS2 plasmid containing FseI and Ascl sites downstream of the Kozak sequence followed by a sequence for the 6 Myc tags in tandem. Respective mutant constructs lacking the putative PKA target serine/threonine residues were generated by site-directed mutagenesis (see below). The amino acid boundaries for mouse Gli2/Gli3 fragments were as follows: Gli3: Pa – 145-216, Pb – 207-237, Pc-g – 259-323, Ph – 312-346, Pi,j – 379-480, P1-4 – 837-922, Pk – 915-978, P5,6 – 965-1018, Pl – 1007-1042, Pm-o – 1510-1577, Gli2 Pc-g – 201-258.

For generation of stable cell lines and for Gli2/3 activity assays, full-length mouse Gli2 and Gli3 sequences were amplified by PCR and cloned into the pENTR2B vector (Life Technologies). Subsequently, a triple HA tag was inserted in-frame on the N-terminus of both constructs and a FLAG tag was added to the C-terminus of the mGli3 construct. These constructs were used for PCR/DpnI-based site-directed mutagenesis (the QuikChange method). Alternatively, large fragments containing multiple mutations were created by gene synthesis (Integrated DNA Technologies) and inserted into the WT plasmid by restriction enzyme-based cloning. The WT and mutant variants of Gli protein genes were shuttled into the pEF5/FRT/V5-DEST using Gateway cloning (Life Technologies).

For *in ovo* electroporation assays, full length Gli2 constructs were subcloned using PCR from the pENTR2B-based plasmids described above into the pCIG vector (Megason and McMahon, 2002), which contains the IRES-GFP cassette. From these plasmids, each Gli2 sequence including the IRES-GFP cassette was cloned into the pECE vector containing an early SV40 promoter (Ellis et al., 1986).

## Transfection

The FuGene 6 reagent (Roche) was used for transient and stable transfections of plasmids into the NIH/3T3-derived lines according to the manufacturer's instructions.

Lipofectamine RNAiMAX (Life Technologies) was used for RNAi transfections. The calcium phosphate method was used for transfection of 293T cells.

## In-vitro phosphorylation

Myc-tagged Gli2/3 fragments were cloned into pCS2 and overexpressed in HEK 293T cells. They were immunoprecipitated overnight from RIPA buffer (50 mM Tris, pH 7.4, 150mM NaCl, 2% NP-40, 0.25% sodium deoxycholate, 1mM DTT, protease and phosphatase inhibitors) lysates using Dynabeads Protein G (Life Technologies) coupled to the goat anti-Myc antibody (Bethyl). *In vitro* phosphorylation was carried out in the PKA reaction buffer (50mM Tris pH 7.5, 10mM MgCl<sub>2</sub>, 0.1% NP-40, 1mM DTT) in the presence of 0.5mM ATP, 10 $\mu$ Ci of [ $\gamma$ -<sup>32</sup>P]ATP, and 21 units of PKA (NEB) for 30 min at 30°C and stopped by washing the beads in ice-cold 50mM Tris pH 7.5, 0.1% NP-40. Protein was eluted off beads using 2x SDS sample buffer and resolved on a 12% SDS-PAGE gel. The protein was transferred onto nitrocellulose membranes, which were air-dried and exposed to Phosphor Screens for quantification of radioactivity using a Typhoon Imager (GE). The membranes were then processed for western blotting with an anti-Myc antibody to assay the total amount of each fragment.

## Sequence analysis

Multiple sequence alignment was carried out using Geneious Pro using the Geneious global alignment protocol with the Blosom62 cost matrix, free end gaps, gap open penalty of 12, and gap extension penalty of 3.

### **Hedgehog reporter luciferase assay**

NIH/3T3 Flp-In cells were seeded into 24-well plates at a density of  $10^5$  cells/well and co-transfected 1-2 hours later with the indicated amounts of the mGli2/mGli3 construct and two luciferase plasmids: pRL-TK containing the renilla luciferase under the constitutive thymidine kinase promoter, and a plasmid containing firefly luciferase driven by octameric Gli binding sites (Sasaki et al., 1997). After reaching confluence the cells were serum-starved and treated for 18-24h with vehicle or 100nM SAG. The cells were harvested and the luciferase assay was performed using the Dual Luciferase Reporter Assay System (Promega) according to the manufacturer's instructions on a BioTek H1 plate reader. All luminescence values were background-corrected using readouts from untransfected cell lysates. For each sample, to control for transfection efficiency, the firefly luciferase luminescence value (Hh-dependent) was divided by the renilla luciferase luminescence value (Hh-independent) to obtain relative luminescence units (RLU). These were then normalized to RLU values obtained from samples that were only transfected with the two luciferase plasmids and not treated with any drugs, yielding fold increase over control. In this assay, the over-expressed Gli proteins are not responsive to Hh ligands, and so their intrinsic transcriptional potential can be gauged. Each experiment was repeated at least three times with similar results.

### **SDS-PAGE and quantitative western blotting**

Cells were harvested in PBS and lysed in RIPA buffer (see above) containing protease and phosphatase inhibitors. Protein concentration was measured using BCA and equal amounts of protein for each sample was mixed with 2x sample buffer and run on 8-12% polyacrylamide gels. The protein was transferred to nitrocellulose and the membranes were blotted with the appropriate primary antibodies followed by secondary antibodies conjugated to infrared dyes (IRDye™). Sixteen-bit images generated from these blots were used for quantification of all protein bands (ImageJ). This pipeline allowed accurate quantification of protein levels on immunoblots across a much wider dynamic range compared to the use of HRP-conjugated

secondary antibodies and conventional film. The primary antibodies used for western blotting were as follows: mouse anti-Gli1 (L42B10, Cell Signaling), guinea pig anti-Gli2 (antigen made in-house based on Cho et al., 2008, sera generated by Cocalico Biologicals, affinity-purified in-house), mouse anti-HA (clone 16B12, Covance), mouse anti- $\alpha$ -tubulin (Sigma), rabbit anti-lamin A (Abcam), goat anti-Myc (Bethyl Labs), rabbit anti-Sufu (made in-house – Humke et al., 2010), anti-pan-14-3-3 (clone K19, Santa Cruz).

### **Quantitative real-time RT-PCR (qPCR)**

RNA was harvested from cells using the TRIzol reagent (Life Technologies) according to manufacturer's instructions. cDNA was generated using the iScript Supermix (Bio-Rad). qPCR reactions were run using the iTaq SYBR green Supermix (Bio-Rad) on the Applied Biosystems 7900HT Fast real-time PCR system. Data were analyzed using the standard curve method with GAPDH used as the housekeeping gene for normalization of mRNA levels in all cases. The following primers were used: GAPDH fwd.: GGCCTTCCGTGTTCTAC, GAPDH rev.: TGTCATCATACTTGGCAGGTT, Gli1 fwd.: CCAAGCCAACTTTATGTCAGGG, Gli1 rev.: AGCCCGCTTCTTTGTTAATTTGA, HA-Gli2 (tagged protein-specific) fwd.: CGCGGTACCAAGCGGAGGAA, HA-Gli2 rev.: TGGGTCGGGGAAGCTGCTGT. All plots are mean +/- standard deviation.

### **Immunohistochemistry/in situ hybridization of chick tissue**

Spinal cords were collected, fixed for 1 hour in 4% PFA at 4°C, cryoprotected in 30% sucrose overnight, mounted in OCT, cut into 12 $\mu$ m thick sections, and collected directly onto slides. To observe the progenitor domains that make up the developing spinal cord the following antibodies were used: rabbit anti-OLIG2 (Millipore); sheep anti-GFP (Biogenesis); rabbit anti-GFP (Invitrogen); mouse anti-FOXA2, mouse anti-NKX2.2, mouse anti-NKX6.1, mouse anti-PAX6, and mouse anti-PAX7 (Developmental Studies Hybridoma Bank); rabbit anti-FOXA2 (Weinstein et al., 1994). In addition, Alexa488-, FITC-, Cy3- and Cy5-conjugated secondary antibodies were obtained from Jackson ImmunoResearch. Fluorescence images were collected

using a Zeiss LSM5 Exciter confocal imaging system and processed using ImageJ. The constructs used for electroporation alone were: pECE-Gli2-IRES-GFP, pECE-Gli2P1-4A-IRES-GFP, pECE-Gli2P1-6A-IRES-GFP. For co-electroporation with mPtc<sup>Δloop2</sup>-IRES-GFP (Briscoe et al., 2001), the pECE plasmids were replaced with the respective pCIG plasmids. Gli2-IRES-GFP and mPtc<sup>Δloop2</sup>-IRES-GFP constructs were electroporated at a final ratio of 1:4 (0.125 μg/μl Gli2 + 0.5 μg/μl mPtc<sup>Δloop2</sup>).

For in situ hybridization, digoxigenin (DIG)-labeled *PTCH1* antisense probes were prepared by in vitro transcription using a chick *PTCH1* construct (Pearse et al., 2001). Slides were fixed in PFA, digested in Proteinase K, postfixed in PFA, acetylated, and hybridized with DIG-labeled probes overnight at 72°C. After hybridization the slides were washed, blocked, and stained with alkaline phosphatase-conjugated anti-DIG antibodies (Roche) overnight at 4°C. The signal was developed using NBT/BCIP (Roche), and the slides were dried and mounted with coverslips.

### **Selected Reaction Monitoring mass spectrometry**

For harvesting, the cells were rinsed with ice-cold PBS, and lysed directly on the dishes in a buffer containing 100mM NaH<sub>2</sub>PO<sub>4</sub>, 10mM Tris pH 8, 8M urea, and 300mM NaCl. The lysate was sonicated to reduce viscosity and the lysis buffer was diluted to a final urea concentration of 2M with RIPA buffer containing protease and phosphatase inhibitors, as well as 25mM glycinamide hydrochloride and 50mM ammonium chloride. The diluted lysate was cleared by ultracentrifugation and Gli2 was immunoprecipitated for 36h at 4°C using Protein A-linked Dynabeads (Life Technologies) coupled to a rabbit anti-Gli2 antibody (antigen based on Cho et al., 2008, serum produced by Cocalico Biologicals, affinity-purified in-house). Gli2 was eluted for 30 min at 37°C, and the eluate was run on a Novex 8% Tris-Glycine SDS -PAGE gel. The gel was thoroughly washed in water, stained with the GelCode Blue reagent (colloidal Coomassie blue; Thermo Fisher) and destained in water. Gli2 bands were excised from the gel and destained sequentially several times in 50mM AmBic (ammonium bicarbonate) and 50%

acetonitrile (ACN)/25mM AmBic. Gel slices were dehydrated in 100% ACN and dried in a speed-vac. The slices were rehydrated in 50mM AmBic containing 5ng/μL of sequencing-grade trypsin (Promega) and overlaid with 50mM AmBic. Digestion was performed overnight at 37°C. The digested peptides were extracted from the gel several times with 5% formic acid and a solution containing heavy peptide standards was added to the peptide mixture. The peptides were purified with the Waters Oasis μElution HLB 96-well plate (30μm particle size) according to the manufacturer's instructions and evaporated to dryness in a speed-vac. They were then resuspended in 2%ACN, 0.1% formic acid (Sigma, HPLC grade), sonicated, and loaded onto a nano HPLC system for separation and MS analysis.

A Proxeon nanospray ionization source was used to interface between an EASY-nLC Nano-HPLC system (Proxeon, Odense, Denmark) and a TSQ Vantage triple quadrupole MS system (Thermo Fisher Scientific, Bremen, Germany). Peptide separation was carried out using a 35 mm x 0.1 mm C18 trapping column (MICHROM C18, 5 μm, 120 Å) and a 200mm x 0.075 mm diameter reverse-phase C18 capillary column (Maisch C18, 3μm, 120 Å). Peptides were separated with a linear gradient from 5% to 45% acetonitrile in 70 min, at a flow rate of 300 nl/min. For all MS experiments, the following parameters were used: positive polarity, Q1 and Q3 both set to 0.70 u (FWHM), emitter voltage set to 1500 V, and the temperature of the transfer capillary set to 270°C. Scheduled SRM was carried out using a maximum window of 5 min, a cycle time of 1s, and an average dwell time of 26 ms. To verify proper operating performance and to determine if the LC/MS system needed cleaning or calibration standard peptide mixture (6 Bovine Protein Digest Equal Molar Mix, MICHROM, USA) was injected into the mass spectrometer at regular intervals between batches of samples and analyzed in SRM mode.

For each monitored peptide, a synthetic heavy arginine-labeled version was spiked into the tryptic digest to provide an internal standard for each SRM run. SRM traces were imported as raw data into Skyline version 1.4 and analyzed. Peptides were quantified by taking a ratio of

areas under the curve of extracted ion currents for each light and heavy peptide and normalizing the obtained ratios based on non-phosphorylatable Gli2 tryptic peptides quantified in the same run. Bar graphs are mean +/- standard deviation of 2 independent SRM runs.

Peptides and transitions (precursor/fragment ions) were selected by testing candidate transitions using unscheduled LC/ESI SRM analysis with the following SRM setup: a scan width of 0.002 m/z was used and a scan time 0.02 s was applied, Q1 and Q3 were set to 0.70 FWHM and the collision gas pressure was of 1.5 Torr. After a set of high quality transition were found for each peptide with 3 transitions by which each transition displayed a S/N > 3, the set was validated by a heavy-labeled synthetic version of each peptide. Only if endogenous and the heavy internal standard peptides displayed the same retention time and fragment ion intensity distribution during collision induced fragmentation, were the peptides used for quantification. This was important to ensure that we were monitoring the correct phosphopeptide and not one in which the phosphate moiety was located on a different S/T residue within the same tryptic peptide. If the specific residue phosphorylated were different between the standard and the monitored peptide, this would result in altered chromatographic mobility and changes in fragmentation patterns for this peptide—that is, the peak retention time as well as the relative height of the peaks for various transitions would be different between the heavy-isotope labeled standard and the peptide derived from the sample (Beck et al., 2011).

The heavy peptides were obtained from JPT Peptides (Berlin, Germany). In each peptide, the C-terminal arginine residue was substituted with the corresponding heavy isotope-labeled version resulting in a mass shift of +10 Da. The peptide transitions in heavy and light versions were measured using scheduled SRM. The transitions monitored are listed in Table S1.

### **Immunoprecipitation/western blot**

For HA tag immunoprecipitation the anti-HA agarose (high affinity; Roche) was used. Elution was carried out in 1x SDS sample buffer at 37°C for 30 min and the eluate was loaded directly on gel.

### **Data normalization**

In Hh reporter assay using transient expression of Gli variants, all values for the Gli-induced firefly luciferase activity were normalized to the activity of a co-transfected renilla luciferase enzyme expressed under a constitutive thymidine kinase promoter to account for well-to-well variability in transfection efficiencies.

For immunoblot experiments, band intensities derived from densitometry were normalized to intensities of a loading control band (tubulin or lamin) from the same lane. In addition, where appropriate, levels of Gli1 protein or mRNA, which was taken as a metric for the transcriptional activity of HA-Gli2 variants, was normalized to the band intensity of the corresponding HA-Gli2 variant to calculate the specific activity (Gli1 activation per unit of HA-Gli2). This normalization method accounts for differences in HA-Gli2 protein expression between the different cell lines, allowing a comparison of the intrinsic transcriptional activity of each HA-Gli2 variant.

In real-time qRT-PCR experiments, all gene expression values were corrected for variability in mRNA loading and PCR efficiency using the standard curve method with GAPDH acting as the housekeeping gene. To calculate the specific activity of each mutant HA-Gli2 protein, Gli1 mRNA values (Figures 3D and 3E) obtained from the standard curve method were normalized to the corresponding HA-Gli2 protein levels from separate immunoblot experiments (Figure 3C).

Mass spectrometric results of phosphopeptide abundance were normalized both to the peak intensity of the corresponding heavy isotope-labeled standard peptide spiked into the tryptic digest at a constant concentration and to the mean of relative intensities of two non-

phosphorylatable “loading control” Gli2 tryptic peptides present in the same sample. This second operation ensured that sample-to-sample variability in protein harvesting, tryptic digest, and extraction of peptides from the gel did not affect the quantification of phosphopeptide abundance.

## SUPPLEMENTAL REFERENCES

- Asaoka, Y., Kanai, F., Ichimura, T., Tateishi, K., Tanaka, Y., Ohta, M., Seto, M., Tada, M., Ijichi, H., Ikenoue, T., et al. (2010). Identification of a suppressive mechanism for Hedgehog signaling through a novel interaction of Gli with 14-3-3. *J. Biol. Chem.* *285*, 4185–4194.
- Beck, F., Lewandrowski, U., Wiltfang, M., Feldmann, I., Geiger, J., Sickmann, A., and Zahedi, R.P. (2011). The good, the bad, the ugly: validating the mass spectrometric analysis of modified peptides. *Proteomics* *11*, 1099–1109.
- Canettieri, G., Di Marcotullio, L., Greco, A., Coni, S., Antonucci, L., Infante, P., Pietrosanti, L., De Smaele, E., Ferretti, E., Miele, E., et al. (2010). Histone deacetylase and Cullin3-REN(KCTD11) ubiquitin ligase interplay regulates Hedgehog signalling through Gli acetylation. *Nat. Cell Biol.* *12*, 132–142.
- Chinchilla, P., Xiao, L., Kazanietz, M.G., and Riobo, N.A. (2010). Hedgehog proteins activate pro-angiogenic responses in endothelial cells through non-canonical signaling pathways. *Cell Cycle Georget. Tex* *9*, 570–579.
- Cho, A., Ko, H.W., and Eggenschwiler, J.T. (2008). FKBP8 cell-autonomously controls neural tube patterning through a Gli2- and Kif3a-dependent mechanism. *Dev. Biol.* *321*, 27–39.
- Cox, B., Briscoe, J., and Ulloa, F. (2010). SUMOylation by Pias1 regulates the activity of the Hedgehog dependent Gli transcription factors. *PLoS One* *5*, e11996.
- Ellis, L., Clauser, E., Morgan, D.O., Edery, M., Roth, R.A., and Rutter, W.J. (1986). Replacement of insulin receptor tyrosine residues 1162 and 1163 compromises insulin-stimulated kinase activity and uptake of 2-deoxyglucose. *Cell* *45*, 721–732.
- Gsponer, J., Futschik, M.E., Teichmann, S.A., and Babu, M.M. (2008). Tight regulation of unstructured proteins: from transcript synthesis to protein degradation. *Science* *322*, 1365–1368.
- Linding, R., Jensen, L.J., Diella, F., Bork, P., Gibson, T.J., and Russell, R.B. (2003). Protein disorder prediction: implications for structural proteomics. *Struct. Lond. Engl.* *1993* *11*, 1453–1459.
- Low, W.-C., Wang, C., Pan, Y., Huang, X.-Y., Chen, J.K., and Wang, B. (2008). The decoupling of Smoothed from Galphai proteins has little effect on Gli3 protein processing and Hedgehog-regulated chick neural tube patterning. *Dev. Biol.* *321*, 188–196.
- Di Marcotullio, L., Ferretti, E., Greco, A., De Smaele, E., Screpanti, I., and Gulino, A. (2007). Multiple ubiquitin-dependent processing pathways regulate hedgehog/gli signaling: implications for cell development and tumorigenesis. *Cell Cycle Georget. Tex* *6*, 390–393.
- Megason, S.G., and McMahon, A.P. (2002). A mitogen gradient of dorsal midline Wnts organizes growth in the CNS. *Dev. Camb. Engl.* *129*, 2087–2098.
- Mukhopadhyay, S., Wen, X., Ratti, N., Loktev, A., Rangell, L., Scales, S.J., and Jackson, P.K. (2013). The Ciliary G-Protein-Coupled Receptor Gpr161 Negatively Regulates the Sonic Hedgehog Pathway via cAMP Signaling. *Cell* *152*, 210–223.
- Ogden, S.K., Fei, D.L., Schilling, N.S., Ahmed, Y.F., Hwa, J., and Robbins, D.J. (2008). G protein Galphai functions immediately downstream of Smoothed in Hedgehog signalling. *Nature* *456*, 967–970.
- Oosterveen, T., Kurdija, S., Alekseenko, Z., Uhde, C.W., Bergsland, M., Sandberg, M., Andersson, E., Dias, J.M., Muhr, J., and Ericson, J. (2012). Mechanistic differences in the

transcriptional interpretation of local and long-range Shh morphogen signaling. *Dev. Cell* 23, 1006–1019.

Pearse, R.V., 2nd, Vogan, K.J., and Tabin, C.J. (2001). Ptc1 and Ptc2 transcripts provide distinct readouts of Hedgehog signaling activity during chick embryogenesis. *Dev. Biol.* 239, 15–29.

Polizio, A.H., Chinchilla, P., Chen, X., Kim, S., Manning, D.R., and Riobo, N.A. (2011). Heterotrimeric Gi proteins link Hedgehog signaling to activation of Rho small GTPases to promote fibroblast migration. *J. Biol. Chem.* 286, 19589–19596.

Shen, F., Cheng, L., Douglas, A.E., Riobo, N.A., and Manning, D.R. (2013). Smoothed is a Fully Competent Activator of the Heterotrimeric G Protein Gi. *Mol. Pharmacol.*

Sheng, T., Chi, S., Zhang, X., and Xie, J. (2006). Regulation of Gli1 localization by the cAMP/protein kinase A signaling axis through a site near the nuclear localization signal. *J. Biol. Chem.* 281, 9–12.

Weinstein, D.C., Ruiz i Altaba, A., Chen, W.S., Hoodless, P., Prezioso, V.R., Jessell, T.M., and Darnell, J.E., Jr (1994). The winged-helix transcription factor HNF-3 beta is required for notochord development in the mouse embryo. *Cell* 78, 575–588.

Xue, B., Dunbrack, R.L., Williams, R.W., Dunker, A.K., and Uversky, V.N. (2010). PONDR-FIT: a meta-predictor of intrinsically disordered amino acids. *Biochim. Biophys. Acta* 1804, 996–1010.